

Impact of leptonic unitary and DM direct detection experiments on sneutrino DM sector in the NMSSM with inverse seesaw mechanism

Junjie Cao^{a,b}, Yangle He^a, Yusi Pan^a, Yuanfang Yue^a, Haijing Zhou^a, Pengxuan Zhu^a

^a *Department of Physics, Henan Normal University, Xinxiang 453007, China*

^b *Center for High Energy Physics, Peking University, Beijing 100871, China*

E-mail: junjiecao@alumni.itp.ac.cn, heyangle@htu.edu.cn,
panyusi0406@foxmail.com, yuanfang405@gmail.com,
zhouhaijing0622@163.com, zhupx99@icloud.com

ABSTRACT: In the Next-to-Minimal Supersymmetric Standard Model with inverse seesaw mechanism for neutrino mass, the lightest sneutrino may act as a feasible DM candidate in broad parameter space. In this case, the smallness of the unitary violation in neutrino sector and the recent XENON-1T experiment are able to limit the DM sector, especially they can set upper bounds on neutrino Yukawa couplings λ_ν and Y_ν . We study such an effect by encoding the constraints in a likelihood function and then performing elaborated scans over the vast parameter space of the theory by Nested Sampling algorithm. We show that the constraints are complementary to each other in limiting the theory, and in some cases they are rather tight. We also study the impact of future LZ experiment on the theory.

Contents

1	Introduction	1
2	NMSSM with inverse seesaw mechanism	3
2.1	Model Lagrangian	3
2.2	Unitary Constraints	4
2.3	Sneutrino DM	6
2.4	DM-nucleon Scattering	9
3	Constraints on the DM sector	11
3.1	Research strategy	12
3.2	Results for light h_s scenario	14
3.3	Results for heavy h_s scenario	20
4	Conclusion	23

1 Introduction

As the most popular ultraviolet-complete Beyond Standard Model, the Minimal Supersymmetric Standard Model (MSSM) with R-parity conservation predicts two kinds of electric neutral, possibly stable and weakly interactive massive particles, namely sneutrino and neutralino, which may act as dark matter (DM) candidates [1, 2]. In the 1990s, it was proven that the left-handed sneutrino as the lightest supersymmetric particle (LSP) predicts a much smaller relic abundance than its measured value as well as an unacceptably large DM-nucleon scattering rate due to its interaction with Z boson [3, 4]. This fact made the lightest neutralino (usually with Bino field as its dominant component) the only reasonable DM candidate so that it has been studied intensively since then. However, with the rapid progress in DM direct detection (DD) experiments in recent years, the candidate becomes more and more tightly limited by the experiments [5–8] assuming that it is fully responsible for the measured relic density and that the Higgsino mass μ is less than about 300GeV, which is favored to predict Z boson mass in a natural way [9]. These conclusions apply to the Next-to-Minimal Supersymmetric Standard Model (NMSSM) [10–12], where sneutrinos are pure left-handed and the lightest neutralino as a DM candidate may be either Bino or Singlino dominated [13]. In this context, we revive the idea of sneutrino DM in a series of works [8, 14–16]. Especially, motivated by the phenomenology of neutrino oscillation, we augment the NMSSM with inverse seesaw

mechanism by introducing two types of gauge singlet chiral superfields $\hat{\nu}_R$ and \hat{X} for each generation matter, which have lepton number -1 and 1 respectively and their fermion components are called heavy neutrinos in literatures, and discuss whether the $\tilde{\nu}_R$ (the scalar component of $\hat{\nu}_R$) or \tilde{x} (the scalar component of \hat{X}) dominated sneutrino can act as a feasible DM candidate [14]. We are interested in the inverse seesaw mechanism because it is a TeV scale physics to account for the oscillation and may be tested by experiments in near future. We show by both analytic formulas and numerical calculation that the resulting theory (abbreviated as ISS-NMSSM hereafter) is one of the most economic framework to generate neutrino mass and meanwhile to reconcile the DM DD experiments in a natural way [8, 14].

It is well known that the introduction of the singlet field \hat{S} in the NMSSM can solve the μ problem of the MSSM [13], enhance the theoretical prediction of the SM-like Higgs boson mass [17–19] as well as enrich the phenomenology of the NMSSM (see for example [20–25]). In the ISS-NMSSM, the \hat{S} field also plays extraordinary roles in generating the mass of the heavy neutrinos by the Yukawa interaction $\lambda_\nu \hat{S} \hat{\nu}_R \hat{X}$ and making the sneutrino DM compatible with various measurements [14]. The latter role can be understood from at least two aspects. One is that the newly introduced heavy neutrino superfields are singlets under the gauge group of the SM model, so they can couple directly with \hat{S} by the Yukawa couplings [14]. In this case, the sneutrino DM candidate $\tilde{\nu}_1$, the singlet dominated scalars h_s , A_s as well as the heavy neutrinos ν_h compose a roughly secluded DM sector where the correct DM relic abundance is acquired by the annihilations $\tilde{\nu}_1 \tilde{\nu}_1^* \rightarrow A_s A_s, h_s h_s$ and/or $\tilde{\nu}_1 \tilde{\nu}_1^* \rightarrow \nu_h \bar{\nu}_h$, which may proceed by quartic scalar interactions, s -channel exchange of h_s and t/u -channel exchange of sneutrinos or Singlino. Since this sector communicates with the SM sector mainly by the small singlet-doublet Higgs mixing, the scattering of the DM with nucleons is naturally suppressed, which coincides with current DM DD results. The other is that the singlet Higgs field can mediate the transition between $\tilde{\nu}_1$ pair and the Higgsino pair so that these particles were in thermal equilibrium in early Universe before their freeze-out from the thermal bath. If their mass splitting is less than about 10%, the number density of the Higgsinos can track that of $\tilde{\nu}_1$ during the freeze-out [26] (in literature such a phenomenon was called coannihilation [27]). Since in this case the couplings of $\tilde{\nu}_1$ to SM particles may be very weak, the scattering is again naturally suppressed. We emphasize that in either case the suppression of the scattering prefers a small Higgsino mass, which is involved in the coupling of $\tilde{\nu}_1^* \tilde{\nu}_1$ state to Higgs bosons, and hence there is no tension any more between the naturalness for Z boson mass and DM DD experiments [14].

In the ISS-NMSSM, both the DM annihilation rate and the DM-nucleon scattering rate depend not only on the coupling strength of $\tilde{\nu}_1$ interacting with Higgs fields, i.e. the Yukawa couplings λ_ν and Y_ν (the coefficient for $\hat{\nu}_L \cdot \hat{H}_u \hat{\nu}_R$ interaction) and their corresponding soft breaking trilinear parameters A_{λ_ν} and A_{Y_ν} , but also on Higgs mass spectrum and the mixings among the Higgs fields which are ultimately

determined by the parameters in Higgs sector [14]. As a result, the DM physics is quite complicated, and is difficult to understand in a simple and intuitive way. This inspired us to study its characteristics from different aspects, e.g. from the features of the DM-nucleon scattering [8, 14] and its capability to explain muon anomalous magnetic momentum [28] or other anomaly at the LHC [16]. In this work, we note that large λ_ν and/or Y_ν can enhance significantly the DM-nucleon scattering rate, so they should be limited by the recent XENON-1T experiment [29]. We also note that the upper bound on the unitary violation in neutrino sector sets certain correlation between the couplings λ_ν and Y_ν [30], which in return can limit the parameter space of the ISS-NMSSM. Since these issues were not discussed before, we decide to study the impact of the leptonic unitary and current/future DM DD experiments on sneutrino DM sector. We will show that they are complementary to each other in limiting the theory, and in some cases the constraints are rather tight. Obviously, such a study is helpful to improve the understanding of the theory, and may be taken as the preparation for more comprehensive studies, e.g. a global fit of the theory.

This work is organized as follows. In section 2, we briefly introduce the theory of the ISS-NMSSM. In section 3, we describe the strategy to study the constraints, present numerical results and reveal the underlying physics. Finally, we draw our conclusions in section 4.

2 NMSSM with inverse seesaw mechanism

Since the ISS-NMSSM has been introduced in detail in [8, 14], we only recapitulate its key features in this section.

2.1 Model Lagrangian

The renormalizable superpotential and the soft breaking terms of the ISS-NMSSM take following form [14]

$$\begin{aligned}
W &= \left[W_{\text{MSSM}} + \lambda \hat{s} \hat{H}_u \cdot \hat{H}_d + \frac{1}{3} \kappa \hat{s}^3 \right] + \left[\frac{1}{2} \mu_X \hat{X} \hat{X} + \lambda_\nu \hat{s} \hat{\nu}_R \hat{X} + Y_\nu \hat{l} \cdot \hat{H}_u \hat{\nu}_R \right], \\
L^{\text{soft}} &= \left[L_{\text{MSSM}}^{\text{soft}} - m_S^2 |S|^2 - \lambda A_\lambda S H_u \cdot H_d - \frac{\kappa}{3} A_\kappa S^3 \right] \\
&\quad - \left[m_{\tilde{\nu}}^2 \tilde{\nu}_R \tilde{\nu}_R^* + m_{\tilde{x}}^2 \tilde{x} \tilde{x}^* + \frac{1}{2} B_{\mu_X} \tilde{x} \tilde{x} + (\lambda_\nu A_{\lambda_\nu} S \tilde{\nu}_R^* \tilde{x} + Y_\nu A_{Y_\nu} \tilde{\nu}_R^* \tilde{l} H_u + \text{h.c.}) \right],
\end{aligned}$$

where W_{MSSM} and $L_{\text{MSSM}}^{\text{soft}}$ represent those of the MSSM without the μ -term, terms in the first bracket on the right side of each equation make up the Lagrangian of the NMSSM and those in the second bracket are needed to implement the supersymmetric inverse seesaw mechanism. Note that all the coefficients in the second brackets, i.e. the neutrino mass term μ_X , the Yukawa couplings λ_ν and Y_ν , the soft breaking trilinear coefficients A_{λ_ν} and A_{Y_ν} , the soft breaking parameter B_{μ_X} as well as the

soft breaking masses m_ν^2 and m_x^2 , are 3×3 matrices in flavor space. Also note that, among the parameters in the superpotential, only the matrix μ_X is dimensional. This matrix parameterizes the effect of lepton number violation (LNV), and it may arise from the integration of heavy particles in an ultraviolet high energy theory with LNV interactions (see for example [31–33]). So the magnitude of its elements should be suppressed. Based on similar perspective, one can infer that the matrix B_{μ_X} tends to be small.

Same as the NMSSM, the ISS-NMSSM predicts three CP-even Higgs bosons, two CP-odd Higgs bosons and a pair of charged Higgs bosons. These bosons have following features:

- One CP-even state corresponds to the Higgs boson discovered at the LHC, and if $\tan \beta \gg 1$, it is favored to be $\text{Re}[H_u^0]$ dominated by the LHC data. Note that the mass of the state may be significantly affected by the interaction $\lambda \hat{s} \hat{H}_u \cdot \hat{H}_d$ and/or by doublet-singlet Higgs mixing [17–19]. Throughout this work, we denote this state by h .
- In most cases, the heavy doublet-dominated CP-even state is mainly composed by $\text{Re}[H_d^0]$. It is roughly degenerate in mass with the doublet-dominated CP-odd state, and also with the charged states. The LHC search for extra Higgs bosons and B -physics have required them heavier than about 500 GeV [34]. In the following, we use H , A_H and H^\pm to represent the states.
- With regard to the singlet-dominated states, they may be very light without conflicting with any collider constraints. As we mentioned before, these states may appear as the final state of the sneutrino pair annihilation or mediate the annihilation, and thus play an important role in sneutrino DM physics. These states are labelled by h_s and A_s in this work.

In practice, we take λ , κ , $\tan \beta \equiv v_u/v_d$, A_λ , A_κ and $\mu \equiv \lambda v_s/\sqrt{2}$ as theoretical input parameters of the Higgs sector with $v_u \equiv \sqrt{2}\langle H_u \rangle$, $v_d \equiv \sqrt{2}\langle H_d \rangle$ and $v_s \equiv \sqrt{2}\langle S \rangle$ denoting the vacuum expectation values of the fields H_u , H_d and S respectively.

2.2 Unitary Constraints

In the interaction basis (ν_L, ν_R^*, x) , the neutrino mass matrix is [14]

$$M_{\text{ISS}} = \begin{pmatrix} 0 & M_D^T & 0 \\ M_D & 0 & M_R \\ 0 & M_R^T & \mu_X \end{pmatrix}, \quad (2.1)$$

where the Dirac mass $M_D = \frac{v_u}{\sqrt{2}} Y_\nu$ and the Majorana mass $M_R = \frac{v_s}{\sqrt{2}} \lambda_\nu$ are all 3×3 matrix in flavor space. The matrix M_{ISS} is diagonalized by a 9×9 unitary matrix U_ν

$$U_\nu^* M_{\text{ISS}} U_\nu^\dagger = \text{diag}(m_i, m_{H_j}),$$

to get three light neutrinos and six heavy neutrinos. Without loss of generality, the rotation matrix U_ν^\dagger can be decomposed into the blocks

$$(U_\nu^\dagger)_{9 \times 9} = \begin{pmatrix} U_{3 \times 3} & X_{3 \times 6} \\ Y_{6 \times 3} & Z_{6 \times 6} \end{pmatrix}, \quad (2.2)$$

with $U_{3 \times 3}$ being the submatrix that encodes in the neutrino oscillation information and should be consistent with neutrino experimental results. On the other side, one can also extract the effective mass matrix of the light active neutrinos from Eq.(2.1), which is given by

$$M_{\text{light}} \simeq M_D^T M_R^{T-1} \mu_X M_R^{-1} M_D \equiv F \mu_X F^T \quad (2.3)$$

with $F \equiv M_D^T M_R^{T-1}$. This matrix is diagonalized by the well-known unitary Pontecorvo-Maki-Nakagawa-Sakata (PMNS) matrix

$$U_{\text{PMNS}}^T M_{\text{light}} U_{\text{PMNS}} = \text{Diag}(m_{\nu_1}, m_{\nu_2}, m_{\nu_3}) \quad (2.4)$$

to get the active neutrino mass m_{ν_i} with $i=1, 2, 3$. Generally speaking, due to the mixings among the states (ν_L, ν_R^*, x) , the matrix $U_{3 \times 3}$ in Eq.(2.2) does not overlap with the U_{PMNS} , instead they are related by

$$U_{3 \times 3} \simeq \left(\mathbf{1} - \frac{1}{2} F F^\dagger \right) U_{\text{PMNS}} \equiv (\mathbf{1} - \eta) U_{\text{PMNS}}.$$

In this sense, $\eta \equiv \frac{1}{2} F F^\dagger$ is a measure of the non-unitarity of the matrix $U_{3 \times 3}$, and a global fit to low energy experimental data prefers [35]

$$\begin{aligned} \sqrt{2|\eta|_{ee}} &< 0.050, \quad \sqrt{2|\eta|_{\mu\mu}} < 0.021, \quad \sqrt{2|\eta|_{\tau\tau}} < 0.075, \\ \sqrt{2|\eta|_{e\mu}} &< 0.026, \quad \sqrt{2|\eta|_{e\tau}} < 0.052, \quad \sqrt{2|\eta|_{\mu\tau}} < 0.035, \end{aligned} \quad (2.5)$$

which indicate $U_{\text{PMNS}} \simeq U_{3 \times 3}$ to a good approximation.

From Eq.(2.3), one can express the parameter μ_X in term of the measurements of m_{ν_i} and U_{PMNS} [30, 36]

$$\mu_X = M_R^T m_D^{T-1} U_{\text{PMNS}}^* \text{Diag}(m_{\nu_1}, m_{\nu_2}, m_{\nu_3}) U_{\text{PMNS}}^\dagger m_D^{-1} M_R.$$

This formula indicates that one may set Y_ν and λ_ν to be flavor diagonal, and attribute the neutrino experimental data solely to the non-diagonality of μ_X . In this case, the unitary constraint becomes

$$\left| \frac{[\lambda_\nu]_{11}\mu}{[Y_\nu]_{11}\lambda v_u} \right| > 14.1, \quad \left| \frac{[\lambda_\nu]_{22}\mu}{[Y_\nu]_{22}\lambda v_u} \right| > 33.7, \quad \left| \frac{[\lambda_\nu]_{33}\mu}{[Y_\nu]_{33}\lambda v_u} \right| > 9.4. \quad (2.6)$$

These inequations reveals that the ratio $[\lambda_\nu]_{33}/[Y_\nu]_{33}$ may be significantly smaller than $[\lambda_\nu]_{11}/[Y_\nu]_{11}$ and $[\lambda_\nu]_{22}/[Y_\nu]_{22}$ once λ , μ and v_u (or alternatively $\tan\beta$) are given. Furthermore, if λ_ν is assumed proportional to the identity matrix, $[Y_\nu]_{33}$ may be much larger than $[Y_\nu]_{11}$ and $[Y_\nu]_{22}$.

2.3 Sneutrino DM

In the ISS-NMSSM, if one decomposes the sneutrino fields into CP-even and -odd parts

$$\tilde{\nu}_L = \frac{1}{\sqrt{2}}(\phi_1 + i\sigma_1), \quad \tilde{\nu}_R^* = \frac{1}{\sqrt{2}}(\phi_2 + i\sigma_2), \quad \tilde{x} = \frac{1}{\sqrt{2}}(\phi_3 + i\sigma_3), \quad (2.7)$$

the squared mass of the CP-even fields is given by

$$m_{\tilde{\nu}}^2 = \begin{pmatrix} m_{11} & m_{12} & m_{13} \\ m_{12}^* & m_{22} & m_{23} \\ m_{13}^* & m_{23}^* & m_{33} \end{pmatrix}, \quad (2.8)$$

in the bases (ϕ_1, ϕ_2, ϕ_3) , where

$$\begin{aligned} m_{11} &= \frac{1}{4} \left[2v_u^2 \text{Re}(Y_\nu Y_\nu^*) + 4\text{Re}(m_{\tilde{l}}^2) \right] + \frac{1}{8} (g_1^2 + g_2^2) (-v_u^2 + v_d^2) \mathbf{1}, \\ m_{12} &= -\frac{1}{2} v_d v_s \text{Re}(\lambda Y_\nu^*) + \frac{1}{\sqrt{2}} v_u \text{Re}(Y_\nu A_\nu), \\ m_{13} &= \frac{1}{2} v_s v_u \text{Re}(Y_\nu \lambda_\nu^*), \\ m_{22} &= \frac{1}{4} \left[2v_s^2 \text{Re}(\lambda_\nu \lambda_\nu^*) + 2v_u^2 \text{Re}(Y_\nu Y_\nu^*) + 4\text{Re}(m_{\tilde{\nu}}^2) \right], \\ m_{23} &= \frac{1}{8} \left\{ -2v_d v_u \lambda \lambda_\nu + 2 \left[(-v_d v_u \lambda + v_s^2 \kappa) \lambda_\nu^* + v_s^2 \kappa \lambda_\nu \right] \right. \\ &\quad \left. + \sqrt{2} v_s \left[-4\text{Re}(\mu_X \lambda_\nu^*) + 4\text{Re}(A_{\lambda_\nu}^* \lambda_\nu) \right] \right\}, \\ m_{33} &= \frac{1}{8} \left[4v_s^2 \text{Re}(\lambda_\nu \lambda_\nu^*) + 8\text{Re}(B_{\mu_X}) + 8\text{Re}(\mu_X \mu_X^*) + 8\text{Re}(m_{\tilde{x}}^2) \right]. \end{aligned} \quad (2.9)$$

This matrix can be diagonalized by a unitary matrix V , and consequently the mass eigenstates are $\tilde{\nu}_{R,i} = V_{ij} \phi_j$ with $i, j = 1, 2, 3$. From these formulae, one can learn following facts:

- The squared mass involves a series of 3×3 matrices in flavor space: Y_ν , λ_ν , A_{Y_ν} , A_{λ_ν} , μ_X , B_{μ_X} , $m_{\tilde{l}}$, $m_{\tilde{\nu}}$ and $m_{\tilde{x}}$, and it is a 9×9 matrix in three generation (ϕ_1, ϕ_2, ϕ_3) bases. Among the matrices, only μ_X must be flavor non-diagonal to account for the neutrino oscillation, but since its magnitude is usually less than 10 KeV [36], it can be neglected in calculating sneutrino mass. So in case that there is no flavor mixings for the other matrices, the squared mass is flavor diagonal, and one can work in one generation (ϕ_1, ϕ_2, ϕ_3) bases to simplify the study of the sneutrino DM. In this work we only consider the third generation sneutrinos as DM sector by noting that both the unitary bound and the constraints of the LHC search for sparticles on this sector are significantly weaker than on the other generations [14]. Hereafter when we refer to the parameters

such as Y_ν , λ_ν , etc., we actually denote their 33 elements. Accordingly, the rotation V is understood as a 3×3 chiral mixing matrix. We add that Y_ν and λ_ν can be taken as real and positive numbers by adjusting the phases of the fields $\hat{\nu}_R$ and \hat{X} .

- The mixing of the field ϕ_1 with the other fields is determined by the parameters Y_ν and A_ν , and as Y_ν approaches zero, $|m_{12}|$ and $|m_{13}|$ and consequently $|V_{11}|$ (the left-handed sneutrino component in the lightest sneutrino) will diminish monotonously. In the extreme case of $Y_\nu = 0$, all the quantities vanish and the singlet dominated sneutrinos as mass eigenstates are merely mixtures of ϕ_2 and ϕ_3 . Furthermore, if the first term in m_{22} is far dominant over the rest terms, which can be achieved when the ratio λ_ν/λ is moderately large, and so is m_{33} , we have $m_{22} \simeq m_{33}$. This results in a maximal mixing between ϕ_2 and ϕ_3 fields where the lighter sneutrino state is approximated by $\tilde{\nu}_{R,1} \simeq 1/\sqrt{2}[\phi_2 - \text{Sgn}(m_{23})\phi_3]$ [14]. This is a popular case in the ISS-NMSSM.

In a similar way, one may study the squared mass of the CP-odd sneutrinos in one generation $(\sigma_1, \sigma_2, \sigma_3)$ bases, which is same as Eq.(2.8) except for the substitution $B_{\mu_X} \rightarrow -B_{\mu_X}$. Accordingly, the CP-odd mass eigenstates is given by $\tilde{\nu}_{I,i} = V'_{ij}\sigma_j$ with V' denoting relevant rotation matrix. Since the parameter B_{μ_X} represents the degree of LNV and is theoretically preferred small, we are particularly interested in following two cases:

- The extreme case where $B_{\mu_X} = 0$. In this case, any CP-even sneutrino is accompanied with a mass degenerate CP-odd state. So any mass eigenstate corresponds to a complex field, and it has its anti-particle [37]. As far as the sneutrino DM $\tilde{\nu}_1$ is concerned, we have $\tilde{\nu}_{R,1} \equiv \text{Re}[\tilde{\nu}_1]$, $\tilde{\nu}_{I,1} \equiv \text{Im}[\tilde{\nu}_1]$, $V_{ij} = V'_{ij}$, and $\tilde{\nu}_1$ and its anti-particle $\tilde{\nu}_1^*$ contribute equally to the relic density. This situation is actually a two component DM theory. Note that the $\tilde{\nu}_1^*\tilde{\nu}_1 Z$ coupling in this case is proportional to $|V_{11}|^2$, and it contributes to the scattering of $\tilde{\nu}_1$ with nucleons. This effect is important if V_{11} is not too small (see following discussion). Also note that the $\tilde{\nu}_1^*\tilde{\nu}_1 A_i$ coupling vanishes since it is induced only by the LNV effect.
- A more general case where $|B_{\mu_X}|$ takes a value less than about 100 GeV^2 . This setting results in three features. First, since $m_{\tilde{\nu}_{R,i}} > m_{\tilde{\nu}_{I,i}}$ for $B_{\mu_X} > 0$, the DM candidate $\tilde{\nu}_1$ is identified as $\tilde{\nu}_{I,1}$ state and it has a definite CP number -1. One can reach the opposite conclusion for $B_{\mu_X} < 0$ case. Second, the rotation matrices V and V' are slightly different, and the masses of the CP-even state and its corresponding CP-odd state split by a tiny number, e.g. $|m_{\tilde{\nu}_{R,1}} - m_{\tilde{\nu}_{I,1}}| \simeq 0.2 \text{ GeV}$ for $B_{\mu_X} = 100 \text{ GeV}^2$ and $m_{\tilde{\nu}_{R,1}} \sim 100 \text{ GeV}$. Sneutrino states in such a situation compose a pseudo-complex particle in literatures [33, 38, 39]. Third,

due to the approximate mass degeneracy, $\tilde{\nu}_{R,1}$ and $\tilde{\nu}_{I,1}$ are able to co-annihilate in early universe to get right DM density. Since Z boson couples only to a pair of sneutrino states with opposite CP numbers, it does not contribute to the DM-nucleon scattering any more. Besides, except for the Z funnel region, it also contributes little to the DM annihilation because $\tilde{\nu}_{R,1}\tilde{\nu}_{I,1}Z$ coupling is suppressed by a factor $V_{11}^*V'_{11} \simeq |V_{11}|^2$.

We checked that, as B_{μ_X} varies within the range $|B_{\mu_X}| < 100 \text{ GeV}^2$, the DM density as well as the cross section of current DM annihilation are scarcely changed.

In our study, we fix $B_{\mu_X} = 0$ or $B_{\mu_X} = -100 \text{ GeV}^2$. In either case, the $\tilde{\nu}_1^*\tilde{\nu}_1 h_i$ coupling strength is given by

$$C_{\tilde{\nu}_1^*\tilde{\nu}_1 h_i} = C_{\tilde{\nu}_1^*\tilde{\nu}_1 \text{Re}[H_d^0]} U_{i1} + C_{\tilde{\nu}_1^*\tilde{\nu}_1 \text{Re}[H_u^0]} U_{i2} + C_{\tilde{\nu}_1^*\tilde{\nu}_1 \text{Re}[S]} U_{i3},$$

where $h_i = h_s, h, H, U$ is the matrix to diagonalize the squared mass of CP-even Higgs fields in the bases $s = (\text{Re}[H_d^0], \text{Re}[H_u^0], \text{Re}[S])$, and $C_{\tilde{\nu}_1^*\tilde{\nu}_1 s}$ denotes the coupling of the sneutrino DM pair to the scalar field s , which is given by

$$\begin{aligned} C_{\tilde{\nu}_1^*\tilde{\nu}_1 \text{Re}[H_d^0]} &= \lambda Y_\nu v_s V_{11} V_{12} + \lambda \lambda_\nu v_u V_{12} V_{13} - \frac{1}{4}(g_1^2 + g_2^2) v_d V_{11} V_{11}, \\ C_{\tilde{\nu}_1^*\tilde{\nu}_1 \text{Re}[H_u^0]} &= \lambda \lambda_\nu v_d V_{12} V_{13} - \sqrt{2} Y_\nu A_{Y_\nu} V_{11} V_{12} - Y_\nu^2 v_u V_{11} V_{11} - \lambda_\nu Y_\nu v_s V_{11} V_{13} \\ &\quad - Y_\nu^2 v_u V_{12} V_{12} + \frac{1}{4}(g_1^2 + g_2^2) v_u V_{11} V_{11}, \\ C_{\tilde{\nu}_1^*\tilde{\nu}_1 \text{Re}[S]} &= \lambda Y_\nu v_d V_{11} V_{12} - 2\kappa \lambda_\nu v_s V_{12} V_{13} - \sqrt{2} \lambda_\nu A_{\lambda_\nu} V_{12} V_{13} + \sqrt{2} \lambda_\nu \mu_X V_{12} V_{13} \\ &\quad - \lambda_\nu Y_\nu v_u V_{11} V_{13} - \lambda_\nu^2 v_s (V_{12} V_{12} + V_{13} V_{13}). \end{aligned} \quad (2.10)$$

So far one can learn that, among the parameters in the sneutrino sector, Y_ν , λ_ν , A_{Y_ν} and A_{λ_ν} affect not only the interactions of the sneutrinos, but also the mass spectrum and the mixing of the sneutrinos. In particular, large λ_ν and Y_ν can enhance the coupling strength significantly. By contrast the soft breaking masses m_ν^2 and $m_{\tilde{x}}^2$ affect only the latter property. Given the typical value of the quantities in Eq.(2.10), e.g. $\tan \beta \gg 1$, $|V_{11}| < 0.1$, $Y_\nu, \kappa, \lambda, \lambda_\nu \sim \mathcal{O}(0.1)$ and $\lambda_\nu v_s, \lambda v_s, A_{Y_\nu}, A_{\lambda_\nu} \sim \mathcal{O}(100 \text{ GeV})$, the couplings $C_{\tilde{\nu}_1\tilde{\nu}_1 S}$ can be approximated by

$$\begin{aligned} C_{\tilde{\nu}_1^*\tilde{\nu}_1 \text{Re}[H_d^0]} &\simeq \lambda Y_\nu v_s V_{11} V_{12} + \lambda \lambda_\nu v_u V_{12} V_{13}, \\ C_{\tilde{\nu}_1^*\tilde{\nu}_1 \text{Re}[H_u^0]} &\simeq -\sqrt{2} \lambda_\nu A_{Y_\nu} V_{11} V_{12} - \lambda_\nu Y_\nu v_s V_{11} V_{13} - Y_\nu^2 v_u V_{12} V_{12}, \\ C_{\tilde{\nu}_1^*\tilde{\nu}_1 \text{Re}[S]} &\simeq -2\kappa \lambda_\nu v_s V_{12} V_{13} - \sqrt{2} \lambda_\nu A_{\lambda_\nu} V_{12} V_{13} - \lambda_\nu^2 v_s, \end{aligned} \quad (2.11)$$

with $|C_{\tilde{\nu}_1^*\tilde{\nu}_1 \text{Re}[H_d^0]}|, |C_{\tilde{\nu}_1^*\tilde{\nu}_1 \text{Re}[H_u^0]}| \lesssim 10 \text{ GeV}$ and $C_{\tilde{\nu}_1^*\tilde{\nu}_1 \text{Re}[S]} \lesssim 100 \text{ GeV}$. This estimation reflects the fact that $|C_{\tilde{\nu}_1^*\tilde{\nu}_1 \text{Re}[S]}|$ may be much larger than the other two couplings. The basic reason is that $\tilde{\nu}_1$ is a singlet dominated scalar, so it can couple directly to the field S with the mass dimension of $C_{\tilde{\nu}_1^*\tilde{\nu}_1 \text{Re}[S]}$ induced by v_s or A_{λ_ν} . While

in case of $V_{11} = 0$, the other couplings emerge only after the electroweak symmetry breaking, and their mass dimension originates from v_u .

In the ISS-NMSSM, the sneutrino DM annihilates through following channels to get its measured density [14]:

- (1) $\tilde{\nu}_1 \tilde{H} \rightarrow XY$ and $\tilde{H} \tilde{H}' \rightarrow X'Y'$ with \tilde{H} and \tilde{H}' denoting Higgsino dominated neutralino or chargino, and $X^{(\prime)}$ and $Y^{(\prime)}$ representing any possible SM particles, the heavy neutrinos or the extra Higgs bosons if the kinematics is accessible. This annihilation mechanism is called co-annihilation in literatures [26, 27], and it works only when the mass splitting between \tilde{H} and $\tilde{\nu}_1$ is less than about 10%. This is one of the most important annihilation channels in our study.
- (2) $\tilde{\nu}_1 \tilde{\nu}_1 \rightarrow ss^*$ with s denoting a light Higgs boson, which proceeds through any relevant quartic scalar couplings, the s -channel exchange of a CP-even Higgs boson or the t/u -channel exchange of a sneutrino. This is another important annihilation channel of the DM, and it plays a role when the Yukawa coupling λ_ν or Y_ν is moderately large.
- (3) $\tilde{\nu}_1 \tilde{\nu}_1 \rightarrow \nu_h \bar{\nu}_h$ via the s -channel exchange of a CP-even Higgs boson or the t/u -channel exchange of a neutralino with ν_h denoting a heavy neutrino. This is a distinctive channel in the seesaw extension of the NMSSM.
- (4) $\tilde{\nu}_1 \tilde{\nu}_1 \rightarrow VV^*, Vs, f\bar{f}$ with V and f denoting any gauge boson and fermion in the SM, respectively. This kind of annihilations proceed mainly by the s -channel exchange of CP-even Higgs bosons, and it is important if the Higgs boson is at resonance.
- (5) The annihilations of $\tilde{\nu}'_1$ (the partner of $\tilde{\nu}_1$ with a different CP number) with same final states as those in (2), (3) and (4).

We emphasize that, since $C_{\tilde{\nu}_1^* \tilde{\nu}_1 \text{Re}[S]}$ is potentially large, the channel $\tilde{\nu}_1 \tilde{\nu}_1^* \rightarrow h_s^{(*)} \rightarrow h_i h_j, \nu_h \bar{\nu}_h$ may play an important role in determining the density even when the singlet dominated scalar h_s is far off-shell. We get this conclusion by intensive scans over the parameter space of the ISS-NMSSM, like what we did in the Type-I seesaw extension of the NMSSM [15].

2.4 DM-nucleon Scattering

In case of $B_{\mu_X} \neq 0$, the scattering of $\tilde{\nu}_1$ with nucleon N ($N = p, n$) proceeds by t/u -channel exchange of the CP-even Higgs bosons. Consequently, the spin independent (SI) cross section is given by [14]

$$\sigma_{\tilde{\nu}_1-N}^{\text{SI}} = \frac{F_u^{(N)2} g^2 \mu_{\text{red}}^2 m_N^2}{16\pi m_W^2} \times \left\{ \sum_i \left[\frac{C_{\tilde{\nu}_1^* \tilde{\nu}_1 h_i}}{m_{h_i}^2 m_{\tilde{\nu}_1}} \left(\frac{U_{i2}}{\sin \beta} + \frac{U_{i1}}{\cos \beta} \frac{F_d^N}{F_u^N} \right) \right] \right\}^2,$$

where $\mu_{\text{red}} = m_N/(1 + m_N^2/m_{\tilde{\nu}_1}^2)$ ($N = p, n$) represents the reduced mass of nucleon with $m_{\tilde{\nu}_1}$, $F_u^{(N)} = f_u^{(N)} + \frac{4}{27}f_G^{(N)}$ and $F_d^{(N)} = f_d^{(N)} + f_s^{(N)} + \frac{2}{27}f_G^{(N)}$ are nucleon form factors with $f_q^{(N)} = m_N^{-1} \langle N | m_q q \bar{q} | N \rangle$ and $f_G^{(N)} = 1 - \sum_q f_q^{(N)}$ for $q = u, d, s$ [2]. For the default setting of the package micrOMEGAs [40–42] about nucleon sigma term $\sigma_{\pi N} = 34$ MeV and $\sigma_0 = 42$ MeV [43]¹, one can get $F_u^p \simeq 0.15$ and $F_d^p \simeq 0.14$. Instead if $\sigma_{\pi N} = 59$ MeV [44–46] and $\sigma_0 = 57$ MeV [47] are adopted, the form factors become $F_u^p \simeq 0.16$ and $F_d^p \simeq 0.13$. These results reflect that different choice of $\sigma_{\pi N}$ and σ_0 will induce an uncertainty of $\mathcal{O}(10\%)$ on F_u^p and F_d^p , and it does not change drastically the cross section. Besides, one can also calculate F_q^n by the default setting, and the results are $F_u^n \simeq 0.15$ and $F_d^n \simeq 0.14$. This implies that $\sigma_{\tilde{\nu}_1-p}^{\text{SI}} \simeq \sigma_{\tilde{\nu}_1-n}^{\text{SI}}$ for the Higgs mediated interaction.

In order to illustrate the features of the cross section in a clear way, we consider a special case where $m_{H^\pm} \gtrsim 1\text{TeV}$. For this case, one may first integrate out the heavy doublet Higgs field so that the CP-even Higgs sector contains only the SM Higgs field $\sin \beta \text{Re}[H_u^0] + \cos \beta \text{Re}[H_d^0]$ and the singlet field $\text{Re}[S]$, then calculate the scattering amplitude by mass insertion method. The result takes following form

$$\begin{aligned} \sigma_{\tilde{\nu}_1-N}^{\text{SI}} &\simeq \frac{F_u^{(N)2} g^2 \mu_{\text{red}}^2 m_N^2}{16\pi m_W^2 (125 \text{ GeV})^4} \times \left(\frac{125 \text{ GeV}}{m_h} \right)^4 \times \left(\frac{C_{\tilde{\nu}_1^* \tilde{\nu}_1 \text{Re}[S]}}{m_{\tilde{\nu}_1}} \times \delta \sin \theta \cos \theta \right. \\ &\quad \left. - \frac{\cos \beta C_{\tilde{\nu}_1^* \tilde{\nu}_1 \text{Re}[H_d^0]} + \sin \beta C_{\tilde{\nu}_1^* \tilde{\nu}_1 \text{Re}[H_u^0]}}{m_{\tilde{\nu}_1}} \times (1 + \delta \sin^2 \theta) \right)^2 \\ &\simeq 4.2 \times 10^{-44} \text{ cm}^2 \times \left(\frac{125 \text{ GeV}}{m_h} \right)^4 \times \left(\frac{C_{\tilde{\nu}_1^* \tilde{\nu}_1 \text{Re}[S]}}{m_{\tilde{\nu}_1}} \times \delta \sin \theta \cos \theta \right. \\ &\quad \left. - \frac{\cos \beta C_{\tilde{\nu}_1^* \tilde{\nu}_1 \text{Re}[H_d^0]} + \sin \beta C_{\tilde{\nu}_1^* \tilde{\nu}_1 \text{Re}[H_u^0]}}{m_{\tilde{\nu}_1}} \times (1 + \delta \sin^2 \theta) \right)^2, \end{aligned} \quad (2.12)$$

where $\delta = m_h^2/m_{h_s}^2 - 1$, and θ is the mixing angle of the SM Higgs field and $\text{Re}[S]$ to form mass eigenstates. This formula indicates that if the first or the second term is of order 1, the cross section can reach the sensitivity of the recent XENON-1T experiment [29]. This situation can be achieved only when λ_ν and/or Y_ν are larger than about 0.4 for $m_{\tilde{\nu}_1} = 100$ GeV (see the expression of the coupling $C_{\tilde{\nu}_1^* \tilde{\nu}_1 s}$ in Eq.2.11). We will discuss this issue later.

As for the case of $B_{\mu_X} = 0$ where the DM corresponds to a complex field, Z -boson also mediates the elastic scattering between the DM and nucleon, and thus contributes to the SI cross section. Since the total SI cross section in this case is obtained by averaging over the $\tilde{\nu}_1 N$ and $\tilde{\nu}_1^* N$ scatterings and the interferences between the Z and the Higgs exchange diagrams for the two scattering have opposite

¹Note that in recent years, σ_0 is usually replaced by strangeness-nucleon sigma term $\sigma_s \equiv m_s/(m_u + m_d) \times (\sigma_{\pi N} - \sigma_0) \simeq 12.4 \times (\sigma_{\pi N} - \sigma_0)$ as the input to calculate the nucleon form factor [41]. This may result in a significant difference in the strange quark content in nucleon $f_s^{(N)}$ due to theoretical uncertainties, but as shown in the text, it change little $F_u^{(N)}$ and $F_d^{(N)}$.

sign [48], one can write the SI cross section as [4]

$$\sigma_N^{\text{SI}} \equiv \frac{\sigma_{\tilde{\nu}_1-N}^{\text{SI}} + \sigma_{\tilde{\nu}_1^*-N}^{\text{SI}}}{2} = \sigma_N^h + \sigma_N^Z, \quad (2.13)$$

where σ_N^h is same as before and the Z -mediated contributions are given by

$$\sigma_n^Z \equiv \frac{G_F^2 V_{11}^4}{2\pi} \frac{m_n^2}{(1 + m_n/m_{\tilde{\nu}_1})^2}, \quad \sigma_p^Z \equiv \frac{G_F^2 V_{11}^4 (4 \sin^2 \theta_W - 1)^2}{2\pi} \frac{m_p^2}{(1 + m_p/m_{\tilde{\nu}_1})^2} \quad (2.14)$$

with G_F denoting Fermi constant and θ_W being weak angle. Note that σ_n^Z is larger than σ_p^Z by two order and consequently σ_n^{SI} may differ greatly from σ_p^{SI} . As a result, the effective cross section of the coherent scattering between the DMs and Xenon nucleus (defined as the averaged cross section $\sigma_{\tilde{\nu}_1-Xe}^{\text{SI}}/A^2$ with A denoting the mass number of the Xenon nucleus) takes the form

$$\sigma_{\text{eff}}^{\text{SI}} = 0.169\sigma_p^{\text{SI}} + 0.347\sigma_n^{\text{SI}} + 0.484\sqrt{\sigma_p^{\text{SI}}\sigma_n^{\text{SI}}}, \quad (2.15)$$

where the three coefficients on the right side are acquired by averaging the abundance of different Xenon isotopes in nature. This effective cross section has the property $\sigma_{\text{eff}}^{\text{SI}} = \sigma_N^{\text{SI}}$ if σ_p^{SI} and σ_n^{SI} are equal, and it can be used to compare directly with the bound of the XENON-1T experiment [29].

Before we end the introduction of the theories, we emphasize that the spin dependent cross section of the scattering is always zero, and the SI cross section is usually much smaller than that for neutralino DM in the MSSM and the NMSSM, which was analyzed in detail in Ref.[8, 14]. As a result, the extension is consistent with the XENON-1T experiment in broad parameter space.

3 Constraints on the DM sector

In this section, we study the impact of the leptonic unitary and current/future DM DD experiments on the sneutrino DM sector under the premise that the theory predicts the right density and the photon spectrum of the DM annihilation in dwarf galaxies compatible with the Fermi-LAT observation. In order to illustrate its underlying physics in a clear way, we consider two Higgs scenarios, which are characterised by $m_{h_s} < m_h$ (light h_s scenario) and $m_{h_s} \gg m_h$ (heavy h_s scenario) respectively, by noting that the singlet dominated Higgs boson plays an important role in both the DM annihilations and the DM-nucleon scattering. The reference parameter settings of the scenarios are presented in Table 1, and they are acquired by intensive scan over the parameters in both Higgs sector and sneutrino DM sector with various experimental constraints considered, which is similar to what we did in [15]². We add

²In practice, we have calculated more than ten million samples for each scenario. The settings in Table 1 are among the best ones that are able to fit well with all the experimental data.

Light h_s scenario with $A_\lambda = 2$ TeV						Heavy h_s scenario with $A_\lambda = 2$ TeV					
$\tan \beta$	12.38	λ	0.24	κ	0.23	$\tan \beta$	28.46	λ	0.19	κ	0.60
A_t	2433	A_κ	-680.4	μ	195.2	A_t	2363	A_κ	-120.4	μ	328.0
m_{h_s}	120.4	m_h	125.1	m_H	2332	m_h	125.1	m_{h_s}	2042	m_H	5381
m_{A_s}	608.5	m_{A_H}	2331	m_{H^\pm}	2332	m_{A_s}	592.6	m_{A_H}	5381	m_{H^\pm}	5379
$m_{\tilde{\chi}_1^0}$	186.0	$m_{\tilde{\chi}_2^0}$	-206.1	$m_{\tilde{\chi}_1^\pm}$	197.9	$m_{\tilde{\chi}_1^0}$	318.8	$m_{\tilde{\chi}_2^0}$	-341.3	$m_{\tilde{\chi}_1^\pm}$	333.8
U_{11}	-0.01	U_{12}	-0.29	U_{13}	0.96	U_{11}	-0.04	U_{12}	-1.00	U_{13}	0.003
U_{21}	0.08	U_{22}	0.95	U_{23}	0.29	U_{21}	-0.01	U_{22}	-0.003	U_{23}	-1.00
U_{31}	-1.00	U_{32}	0.08	U_{33}	0.02	U_{31}	1.00	U_{32}	-0.04	U_{33}	-0.01

Table 1. Specific configurations of the Higgs sector for two scenarios discussed in the text. Parameters in mass dimension are in unit of GeV. Other fixed parameters in our study include $m_{\tilde{q}} = 2$ TeV for flavor universal squark soft-breaking masses, $M_1 = M_2 = M_3 = 2$ TeV for gaugino masses, $A_i = 0$ for all trilinear soft-breaking coefficients except for A_λ , A_t , $[A_{Y_\nu}]_{33}$ and $[A_{\lambda_\nu}]_{33}$, as well as $[Y_\nu]_{11,22} = 0.01$, $[\lambda_\nu]_{11,22} = 0.3$, $[m_{\tilde{\nu}}]_{11,22} = [m_{\tilde{x}}]_{11,22} = 2$ TeV for parameters in first two generation sneutrino sector. All the parameters are defined at the scale $Q = 1$ TeV. We remind the fact that the Higgs masses and U_{ij} in this table are obtained by the setting $[Y_\nu]_{33} = [\lambda_\nu]_{33} = 0$, and sneutrino loop effects may slightly change them when one varies the Yukawa couplings.

that, if the exotic decays $h \rightarrow \nu_h \bar{\nu}_h, \tilde{\nu}_1 \tilde{\nu}_1^*$ are kinematically forbidden, the settings are well consistent with the latest data of the LHC about the discovered Higgs boson and the search for extra bosons at the LEP and the LHC. This has been checked with the packages HiggsSignal-2.4.0 [49] and HiggsBounds-5.7.0 [50].

3.1 Research strategy

The procedure of our study is as follows: we first construct the likelihood function for the DM physics, and use it to guide our sophisticated scans over the parameters of the sneutrino sector in either scenario. Then with the samples obtained in the scan, we project the likelihood function on different two dimensional planes to show its features and reveal its underlying physics.

The likelihood function we adopt is composed by

$$\mathcal{L}_{\text{DM}} = \mathcal{L}_{\Omega_{\tilde{\nu}_1}} \times \mathcal{L}_{\text{DD}} \times \mathcal{L}_{\text{ID}} \times \mathcal{L}_{\text{Unitary}}, \quad (3.1)$$

where $\mathcal{L}_{\Omega_{\tilde{\nu}_1}}$, \mathcal{L}_{DD} , \mathcal{L}_{ID} and $\mathcal{L}_{\text{Unitary}}$ account for the relic density, current XENON-1T experiment [29] or future LZ experiment [51], the Fermi-LAT observation of dwarf galaxies, and the unitary constraint in Eq.(2.6) respectively. Their expressions are as follows:

- $\mathcal{L}_{\Omega_{\tilde{\nu}_1}}$ is Gaussian distributed, i.e.

$$\mathcal{L}_{\Omega_{\tilde{\nu}_1}} = e^{-\frac{[\Omega_{\text{th}} - \Omega_{\text{obs}}]^2}{2\sigma^2}}, \quad (3.2)$$

where Ω_{th} denotes the theoretical prediction of the density $\Omega_{\tilde{\nu}_1} h^2$, $\Omega_{\text{obs}} = 0.120$ represents its experimental central value [52] and $\sigma = 0.1 \times \Omega_{\text{obs}}$ is the total (including both theoretical and experimental) uncertainty of the density.

- \mathcal{L}_{DD} takes a Gaussian form with a mean value of zero [53]:

$$\mathcal{L}_{\text{DD}} = e^{-\frac{\sigma_{\tilde{\nu}_1-p}^2}{2\delta_\sigma^2}}, \quad (3.3)$$

where $\sigma_{\tilde{\nu}_1-p}$ stands for the theoretical prediction of the DM-proton scattering rate, δ_σ is evaluated by $\delta_\sigma^2 = UL_\sigma^2/1.64^2 + (0.2\sigma_{\tilde{\nu}_1-p})^2$ with UL_σ denoting the upper limit of relevant DM DD experiment on the scattering cross section at 90% C.L., and $0.2\sigma_{\tilde{\nu}_1-p}$ parameterizing the theoretical uncertainty of $\sigma_{\tilde{\nu}_1-p}$.

- \mathcal{L}_{ID} is calculated by the likelihood function proposed in [54, 55] with the data of the Fermi-LAT collaboration presented in [56, 57].
- For the likelihood function of the unitary constraint in Eq.(2.6), we take following form

$$\mathcal{L}_{\text{Unitary}} = \begin{cases} \exp\left[-\frac{1}{2} \left(\frac{r-9.4}{0.2r}\right)^2\right] & \text{if } r \leq 9.4 \\ 1 & \text{if } r > 9.4 \end{cases} \quad (3.4)$$

with $r \equiv \lambda_\nu \mu / (Y_\nu \lambda v_u)$.

In addition, we abandon samples which open up the decay channel $h \rightarrow \nu_h \bar{\nu}_h$ or $h \rightarrow \tilde{\nu}_1 \tilde{\nu}_1^*$. In practice, this is accomplished by fixing the likelihood value of these samples at e^{-100} .

In order to make the conclusions in this work as complete as possible, we adopt the MultiNest algorithm introduced in [58, 59] to implement the scans. For each scan, we take the prior probability density function (PDF) of the involved input parameters flat distributed, and set the *nlive* parameter of the algorithm, which denotes the number of active or live points used to determine the iso-likelihood contour in each iteration [58, 59], at 10000. Obviously, the larger *nlive* is, the finer the scan becomes. The output of the scan includes the Bayesian evidence, which is generally defined by

$$Z(D|M) \equiv \int P(D|O(M, \Theta)) P(\Theta|M) \prod d\Theta_i,$$

where $P(\Theta|M)$ represents the prior PDF of input parameters $\Theta = (\Theta_1, \Theta_2, \dots)$ in a model M , and $P(D|O(M, \Theta)) \equiv \mathcal{L}(\Theta)$ denotes the likelihood function for the theoretical predictions of the observables O confronted with their experimentally measured values D . Computationally, the evidence is an averaged likelihood, and it depends on the priors of the model's parameters. For different scenarios in one

theory, the larger Z is, the more readily the corresponding scenario is consistent with the data.

With the output of the scan, one can also get the profile likelihood (PL) in frequentist statistics, which is defined as the largest likelihood value in a certain parameter space [15, 60]. Take one dimensional (1D) and two dimensional (2D) PLs as an example, they are acquired by the procedure

$$\begin{aligned}\mathcal{L}(\Theta_A) &= \max_{\Theta_1, \dots, \Theta_{A-1}, \Theta_{A+1}, \dots} \mathcal{L}(\Theta), \\ \mathcal{L}(\Theta_A, \Theta_B) &= \max_{\Theta_1, \dots, \Theta_{A-1}, \Theta_{A+1}, \dots, \Theta_{B-1}, \Theta_{B+1}, \dots} \mathcal{L}(\Theta).\end{aligned}\tag{3.5}$$

Obviously, the PL reflects the preference of a theory on the parameter space, and for any point on 1D direction or 2D $\Theta_A - \Theta_B$ plane, its PL value represents the capability to account for the experimental data by varying the other parameters. Sequentially one can introduce the concept of the confidence interval (CI) to classify the parameter region by the extent that parameter points in it can fit the data. Take the 2D PL as an example, its 1σ and 2σ CIs are defined as the regions satisfying the condition $\chi^2 - \chi_{\min}^2 \leq 2.3$ and $\chi^2 - \chi_{\min}^2 \leq 6.18$ respectively, where $\chi^2 \equiv -2 \ln \mathcal{L}(\Theta_A, \Theta_B)$ and χ_{\min}^2 is the χ^2 value of the best sample in the scan.

In our study, we utilize the package **SARAH-4.11.0** [61–63] to build the model file of the ISS-NMSSM, the codes **SPheno-4.0.3** [64] to generate its particle spectrum, and the package **MicrOMEGAs 4.3.4** [40, 42, 65] to calculate the DM observables.

3.2 Results for light h_s scenario

With the inputs of the Higgs sector in Table 1, the Higgs-mediated SI cross section in Eq.(2.12) is written as

$$\sigma_{\tilde{\nu}_1-N}^{\text{SI}} \simeq 4.2 \times 10^{-44} \text{ cm}^2 \times \left(\frac{0.02 C_{\tilde{\nu}_1^* \tilde{\nu}_1 \text{Re}[S]}}{m_{\tilde{\nu}_1}} + \frac{C_{\tilde{\nu}_1^* \tilde{\nu}_1 \text{Re}[H_u^0]} + 0.08 C_{\tilde{\nu}_1^* \tilde{\nu}_1 \text{Re}[H_d^0]}}{m_{\tilde{\nu}_1}} \right)^2.$$

Given that $C_{\tilde{\nu}_1^* \tilde{\nu}_1 \text{Re}[S]}$ is usually larger than $C_{\tilde{\nu}_1^* \tilde{\nu}_1 \text{Re}[H_u^0]}$ and $C_{\tilde{\nu}_1^* \tilde{\nu}_1 \text{Re}[H_d^0]}$ by two orders for the setting, the first term in the bracket is comparable or even larger than the other terms. In order to investigate the impact of the DM DD experiments on the DM sector, we compare different cases of the scenario by performing four independent scans over following parameters

$$\begin{aligned}0 \leq Y_\nu, \lambda_\nu \leq 0.7, \quad & 0 < m_{\tilde{\nu}}, m_{\tilde{x}} < 500 \text{ GeV}, \\ |A_{Y_\nu}|, |A_{\lambda_\nu}| < 1000 \text{ GeV}, \quad & 400 \text{ GeV} \leq m_{\tilde{l}} \leq 1000 \text{ GeV},\end{aligned}\tag{3.6}$$

where the parameter $m_{\tilde{l}}$ denotes the common soft breaking mass for three generation sleptons. In the first scan, we fix $B_{\mu_X} = -100 \text{ GeV}^2$ and use the upper bound of the XENON-1T experiment on the SI cross section to calculate \mathcal{L}_{DD} . The second scan is similar to the first one except that we use the sensitivity of the future LZ experiment

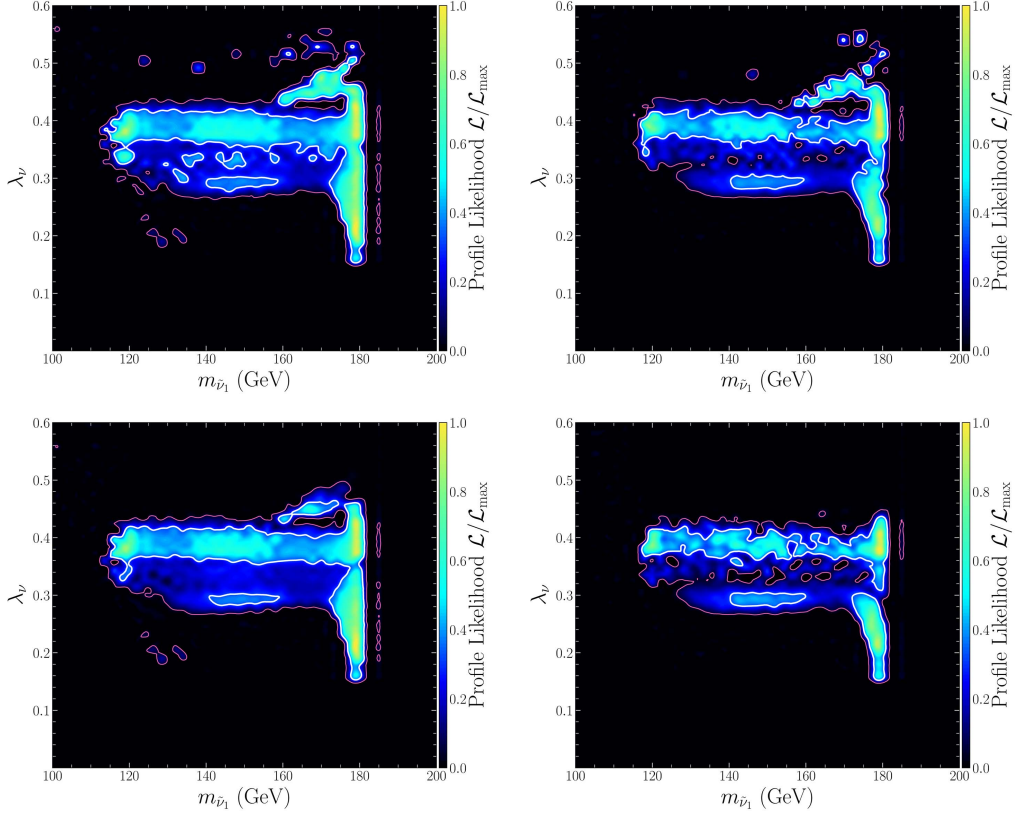


Figure 1. Profile likelihoods of the function \mathcal{L}_{DM} in Eq.(3.1) for the light h_s scenario, which are projected on $\lambda_\nu - m_{\tilde{\nu}_1}$ plane. The upper panels are the results for the case of $B_{\mu_X} \neq 0$ with the bound from the XENON-1T (2018) experiment (left panel) and the future LZ experiment (right panel) on the cross section of the DM-nucleon scattering taken into account in calculating \mathcal{L}_{DM} . The lower panels are obtained in a similar way to the upper panels except that they are for $B_{\mu_X} = 0$ case. Since $\chi^2_{\text{min}} \simeq 0$ for the best point of the scan, the boundary for 1σ confidence interval (white solid line) and that for 2σ confidence interval (red solid line) correspond to $\chi^2 \simeq 2.3$ and $\chi^2 \simeq 6.18$ respectively. This figure reflects the preference of the DM measurements on the parameters λ_ν and $m_{\tilde{\nu}_1}$.

as input of \mathcal{L}_{DD} . The last two scans differ from the previous ones only in that we set $B_{\mu_X} = 0$. As we introduced before, such a setting will induce an additional contribution, namely the Z -mediated contribution, to the DM-nucleon scattering. This will strengthen the constraint of the DD experiments.

With the samples obtained in the scan, we are able to plot the map of the PL for the function \mathcal{L}_{DM} on different planes in Fig.1-5. From Fig.1 and Fig.2 which shows the 1σ and 2σ CIs on $\lambda_\nu - m_{\tilde{\nu}_1}$ and $\sigma_{\tilde{\nu}_1-p}^{\text{SI}} - m_{\tilde{\nu}_1}$ planes respectively, one can learn following facts

- $m_{\tilde{\nu}_1}$ is concentrated on the range from 120 GeV to 181 GeV. For $172 \text{ GeV} \lesssim m_{\tilde{\nu}_1} \lesssim 181 \text{ GeV}$, $m_{\tilde{\nu}_1}$ is close to $m_{\tilde{\chi}_1^0}$ and the DM gets the right density through

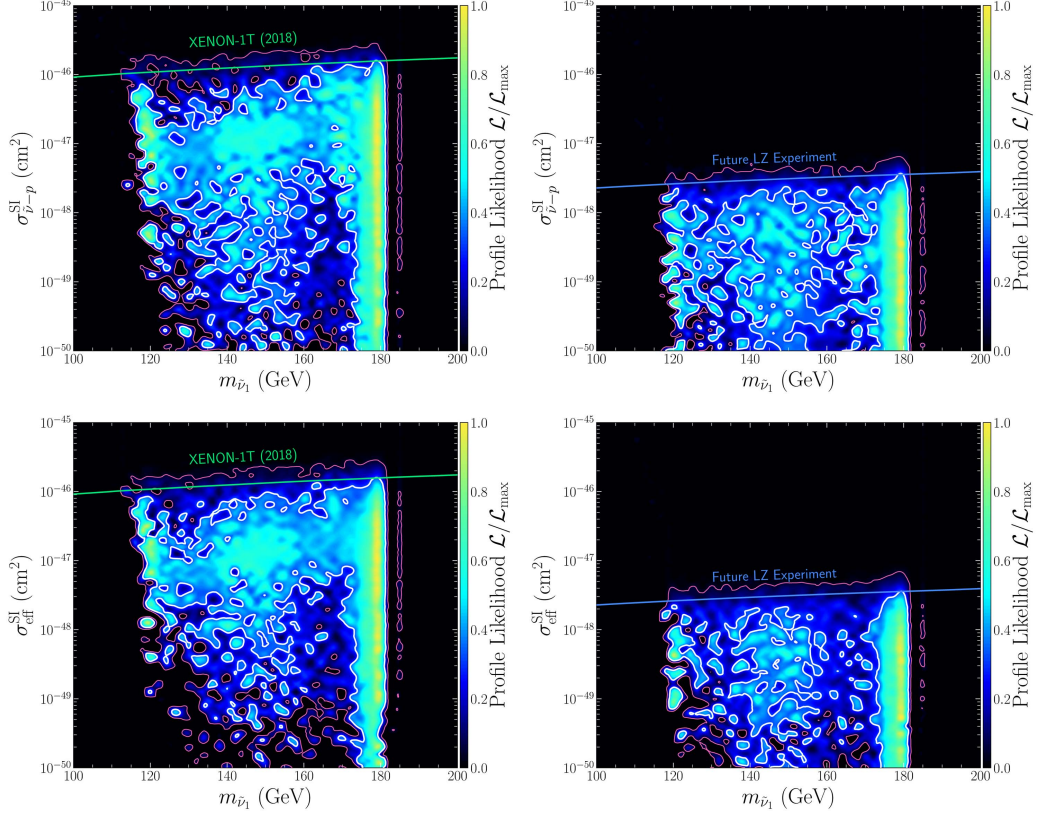


Figure 2. Same as Fig.1, but for the profile likelihood projected on $\sigma_{\tilde{\nu}-p}^{\text{SI}} - m_{\tilde{\nu}_1}$ plane.

its co-annihilation with $\tilde{\chi}_1^0$. In this region, the density is insensitive to the parameter λ_ν , so λ_ν may vary from 0.15 to about 0.6 where the lower bound comes from the requirement $\nu_h > m_h/2$ to forbid kinematically the decay $h \rightarrow \nu_h \bar{\nu}_h$. For the other mass range, the DM achieves its right relic density by the annihilations $\tilde{\nu}_1 \tilde{\nu}_1^* \rightarrow h_s h_s, h_s h, h h$. As indicated by the density formula in [66, 67], λ_ν should be around 0.4 if the scalar quartic interaction $\tilde{\nu}_1^* \tilde{\nu}_1 S S$ is mainly responsible for the density. This feature is shown clearly in Fig.1.

For any mass region, the SI cross section for DM-nucleon scattering may be as low as 10^{-50} cm^2 (see Fig.2). This reflects the general feature that there are multiple mechanism to suppress the scattering so that the cross section is usually preferred small. This feature was recently emphasized in our work [8], and it is also reflected in Eq.(2.12).

- Although we require $\lambda_\nu \leq 0.7$ in the scans, Fig.1 indicates that λ_ν in the 2σ confidence interval (CI) are upper bounded by about 0.56, 0.56, 0.50 and 0.45 for the four scans respectively. By comparing the left panels with corresponding right panels, one can learn that this is due to the constraint of the DM DD experiments on the co-annihilation region. In fact, we compute the Bayesian

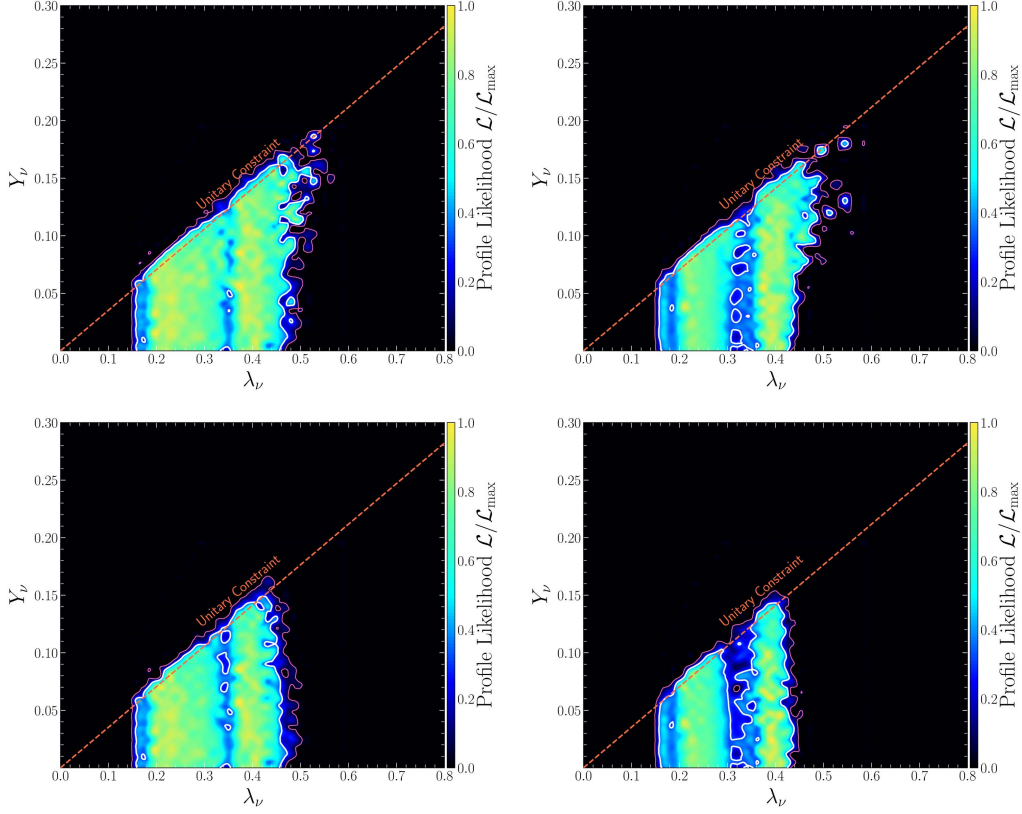


Figure 3. Same as Fig.1, but for the profile likelihood projected on $Y_\nu - \lambda_\nu$ plane with the red line denoting the leptonic unitary bound.

evidences Z_i ($i = 1, 2, 3, 4$) of the scans, and find that $\ln Z_1 = -55.6$, $\delta_{12} \equiv \ln Z_1 - \ln Z_2 = 1.0$, $\delta_{13} \equiv \ln Z_1 - \ln Z_3 = 0.54$ and $\delta_{34} \equiv \ln Z_3 - \ln Z_4 = 1.43$. The Jeffreys' scale δ_{13} [68, 69] reflects the fact that the DM experiments do not show significant preference of the $B_{\mu_X} \neq 0$ case to the $B_{\mu_X} = 0$ case [70]. On the other hand, δ_{12} and δ_{34} indicates that, if the sensitivity of the XENON-1T experiment is improved by 50 times through the LZ experiment, a sizable portion of the parameter space will become disfavored so that the average value of \mathcal{L}_{DM} , namely Bayesian evidence, is lowered by a factor more than 40%. This result is also reflected by the sizable shrink of the 1σ CIs in Fig.1 and Fig.2.

In order to make the implication of Fig.1 clearer, we describe how we get this figure. From Eq.(3.5), one can learn that the 2D PL $\mathcal{L}(\lambda_\nu, m_{\tilde{\nu}_1})$ is given by

$$\mathcal{L}(\lambda_\nu, m_{\tilde{\nu}_1}) = \max_{Y_\nu, A_{\lambda_\nu}, \dots} \mathcal{L}_{\text{DM}}(\lambda_\nu, Y_\nu, A_{\lambda_\nu}, A_{Y_\nu}, m_{\tilde{\nu}}, m_{\tilde{x}}, m_{\tilde{l}}). \quad (3.7)$$

In plotting Fig.1, the maximization over the parameters Y_ν , A_{λ_ν} , A_{Y_ν} , $m_{\tilde{\nu}}$, $m_{\tilde{x}}$ and $m_{\tilde{l}}$ is implemented as follows: we first split the $\lambda_\nu - m_{\tilde{\nu}_1}$ plane into 80×80 equal boxes (i.e. we divide each dimension of the plane by 80 equal bins), then we fit

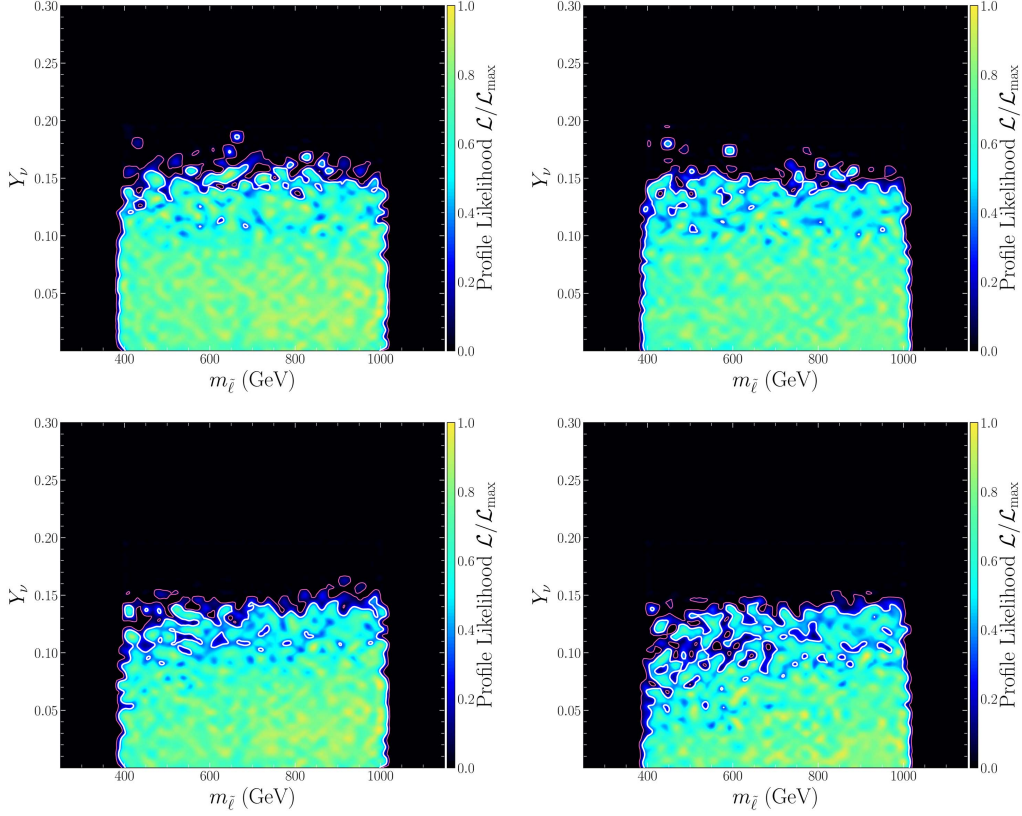


Figure 4. Same as Fig.1, but for the profile likelihood projected on $Y_\nu - m_{\tilde{t}}$ plane.

the samples obtained in the scan into each boxes so that the samples in each box correspond roughly equal λ_ν and $m_{\tilde{\nu}_1}$, but the other parameters may differ greatly. Finally, we pick out the maximum likelihood value from the samples in each box as the PL value. Obviously, $\mathcal{L}(\lambda_\nu, m_{\tilde{\nu}_1})$ obtained in this way reflects the preference of the theory on the parameters λ_ν and $m_{\tilde{\nu}_1}$, and for a given point on $\lambda_\nu - m_{\tilde{\nu}_1}$ plane, its value represents the capability to account for experimental data. We add that $\chi^2_{\min} \simeq 0$ for the best point in the scans. This is because the DM experimental data are independent and consistent with each other, and the ISS-NMSSM can explain well the data.

Next we consider the 2D PL $\mathcal{L}(Y_\nu, \lambda_\nu)$, which is shown in Fig.3 with the red dashed line denoting the correlation $\lambda_\nu \mu / (Y_\nu \lambda v_u) = 9.4$ (or equivalently $\lambda_\nu = 2.9 Y_\nu$) for the unitary constraint. This figure shows that $Y_\nu \lesssim 0.17$ and the upper bound of Y_ν is always determined by the unitary requirement. This feature can be understood as follows: because the unitary constraint has required λ_ν to be several times larger than Y_ν , the SI cross section is much more sensitive to λ_ν than to Y_ν . Consequently λ_ν is upper bounded by the DM DD experiments, while Y_ν is only limited by the unitary constraint.

We also study 2D PLs $\mathcal{L}(Y_\nu, m_{\tilde{t}})$ and $\mathcal{L}(V_{11}, m_{\tilde{t}})$, and plotted their CIs in Fig.4

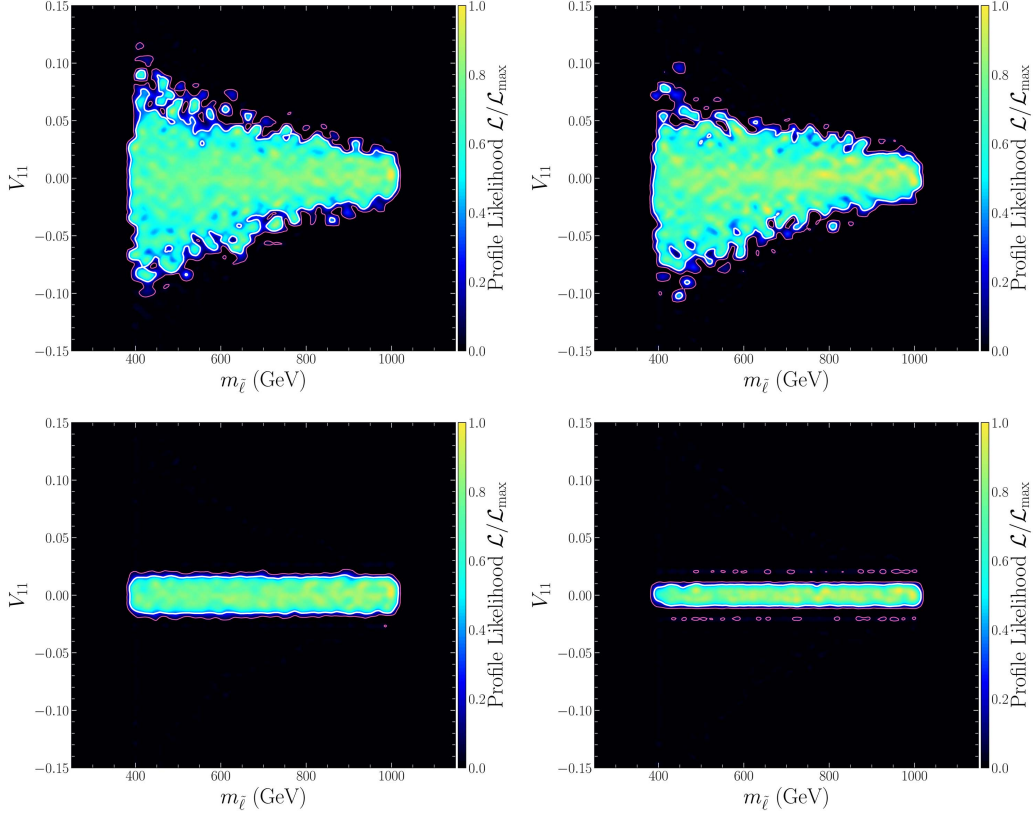


Figure 5. Same as Fig.1, but for the profile likelihood projected on $V_{11} - m_{\tilde{l}}$ plane.

and Fig.5 respectively. Fig.4 indicates that the 2σ CI in each panel forms a rough rectangular area on $Y_\nu - m_{\tilde{l}}$ plane. The basic reason comes from the facts that \mathcal{L}_{DM} relies on $m_{\tilde{l}}$ only through V_{11} and that $|V_{11}|$ is sizable only when Y_ν is relatively large (see the expressions of m_{12} and m_{13} in Eq.2.9). Explicitly speaking, for the $B_{\mu_X} \neq 0$ case V_{11} affects little the annihilation rate and the scattering rate since it is small. This feature together with the moderately weak correlation between the upper bound of $|V_{11}|$ and $m_{\tilde{l}}$ (see the top panels of Fig.5) determines that the favored range of Y_ν is approximately independent of $m_{\tilde{l}}$, which accounts for the rectangular shape. For the $B_{\mu_X} = 0$ case, the effective SI cross section in Eq.(2.15) is mainly contributed by the Z -mediated DM-neutron scattering when V_{11} is sizable, and consequently the maximal value of $|V_{11}|$ favored by the experimental data, especially by the DM DD experiment, is small and independent of $m_{\tilde{l}}$ (see the bottom panels of Fig.5). In this case, one may replace $m_{\tilde{l}}$ by V_{11} as a theoretical input. This again leads to a rough independence of the boundary on $m_{\tilde{l}}$.

Besides, one can learn from Fig.5 that the experiments have required $|V_{11}| \lesssim 0.10$ at 2σ level for the $B_{\mu_X} \neq 0$ case with $m_{\tilde{l}} = 400$ GeV, and that the range becomes narrowed with the increase of $m_{\tilde{l}}$. By contrast, the experimental constraint becomes very tight for the $B_{\mu_X} = 0$ case due to the largeness of the Z -mediated contribution to

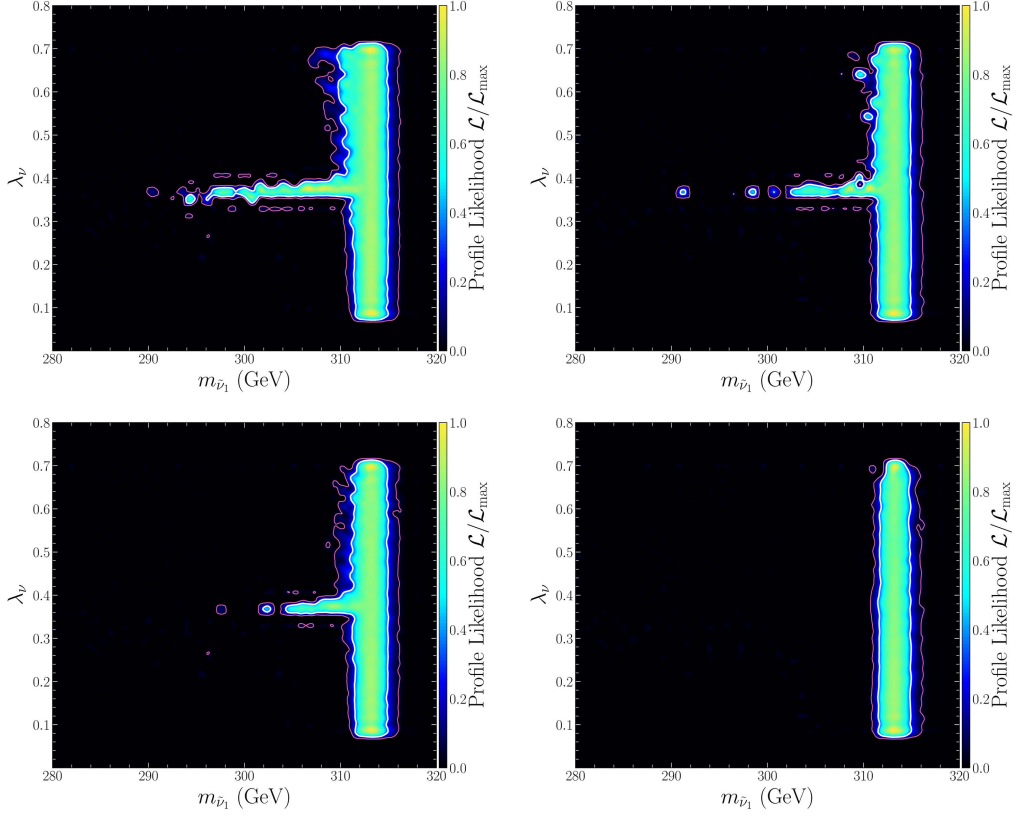


Figure 6. Same as Fig.1, but for the heavy h_s scenario defined in Table 1.

the $\tilde{\nu}_1$ -neutron scattering, i.e. $|V_{11}| \lesssim 0.02$ if the XENON-1T results are considered and $|V_{11}| \lesssim 0.01$ if the future LZ results are adopted. About this conclusion, we coincide with that in [71].

3.3 Results for heavy h_s scenario

In the heavy h_s scenario, the Higgs-mediated SI cross section is given by

$$\sigma_{\tilde{\nu}_1-N}^{\text{SI}} \simeq 4.2 \times 10^{-44} \text{ cm}^2 \times \left(\frac{0.003 C_{\tilde{\nu}_1^* \tilde{\nu}_1 \text{Re}[S]}}{m_{\tilde{\nu}_1}} + \frac{C_{\tilde{\nu}_1^* \tilde{\nu}_1 \text{Re}[H_u^0]} + 0.04 C_{\tilde{\nu}_1^* \tilde{\nu}_1 \text{Re}[H_d^0]}}{m_{\tilde{\nu}_1}} \right)^2,$$

for the parameter setting in Table 1. Given the typical size of $C_{\tilde{\nu}_1^* \tilde{\nu}_1 \text{Re}[S]} \sim \mathcal{O}(10^2 \text{ GeV})$ and $C_{\tilde{\nu}_1^* \tilde{\nu}_1 \text{Re}[H_u^0]}, C_{\tilde{\nu}_1^* \tilde{\nu}_1 \text{Re}[H_d^0]} \sim \mathcal{O}(10 \text{ GeV})$ for $\lambda_{\nu}, Y_{\nu} \gtrsim 0.3$, one can infer that the first term in the bracket is no longer more important than the rest contribution, and $\sigma_{\tilde{\nu}_1-N}^{\text{SI}}$ is of the order 10^{-46} cm^2 in optimal cases for $m_{\tilde{\nu}_1} = 300 \text{ GeV}$ so that the XENON-1T experiment has weak limitation on the $B_{\mu_X} \neq 0$ case of this scenario. This situation is quite different from the light h_s scenario.

Similar to what we did for the light h_s scenario, we perform four independent scans over the parameter space in Eq.(3.6), and project the PL on different planes. The results are presented in Fig.6-10, which correspond to Fig.1-5 respectively. From these figures, one can learn following facts:

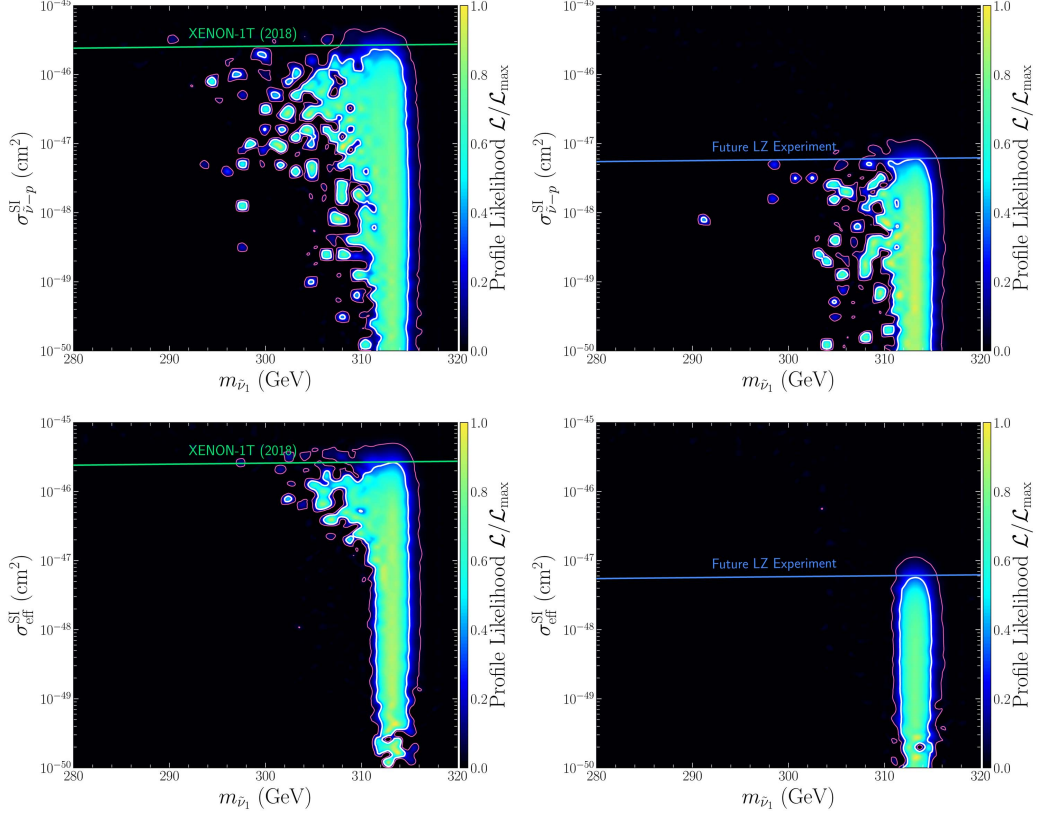


Figure 7. Same as Fig.2, but for the heavy h_s scenario defined in Table 1.

- Since the unitary constraint becomes $\lambda_\nu > 1.3 Y_\nu$ for the setting in Table 1, Y_ν may be comparable with λ_ν . Consequently, the SI cross section is sensitive not only to λ_ν , but also to Y_ν . This feature is different from that of the light h_s scenario.
- Given that the $B_{\mu_X} \neq 0$ case is weakly limited by the XENON-1T experiment, both λ_ν and Y_ν may be larger than 0.4 (see the upper left panel of Fig.8). On the other hand, with the experimental sensitivity improved and/or the Z -mediated contribution added in the $B_{\mu_X} = 0$ case, the DM DD experiments begin to limit λ_ν and Y_ν , and the possibility of $Y_\nu \gtrsim 0.4$ becomes disfavored. This is shown on the rest panels of Fig.8.
- Given $m_{\tilde{\chi}_1^0} \simeq 319$ GeV, $\tilde{\nu}_1$ gets the right density through its co-annihilation with $\tilde{\chi}_1^0$ in most cases, which is shown clearly in Fig.6. Besides, it may also annihilate into hh final state, which proceeds mainly through the $\tilde{\nu}_1^* \tilde{\nu}_1 \text{Re}[H_u^0] \text{Re}[H_u^0]$ interaction for the parameter setting in Table 1. With the formula of the density in [66, 67] and $C_{\tilde{\nu}_1^* \tilde{\nu}_1 \text{Re}[H_u^0] \text{Re}[H_u^0]} = Y_\nu^2 |V_{12}|^2$, one can infer that the right density requires $Y_\nu \gtrsim 0.3$. This expectation coincides with the results in Fig.6 when taking into account the correlation $\lambda_\nu \sim 1.3 Y_\nu$.

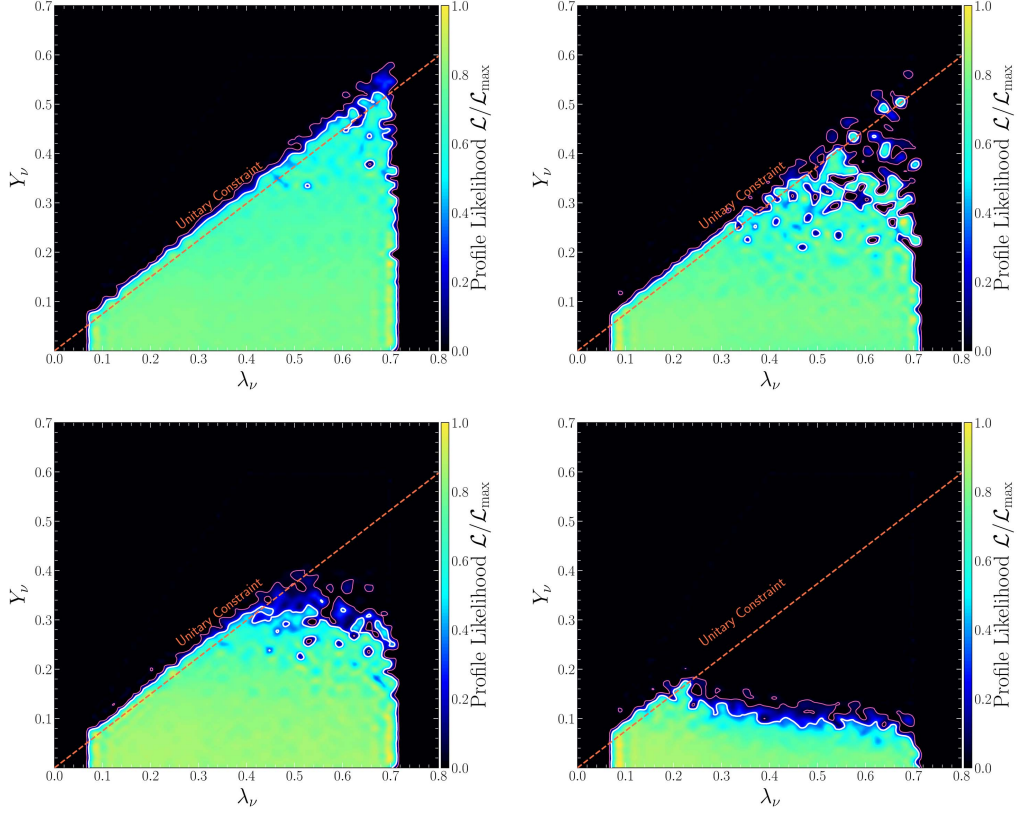


Figure 8. Same as Fig.3, but for the heavy h_s scenario defined in Table 1.

We checked that $\delta_{12} \equiv \ln Z_1 - \ln Z_2 = 0.2$, $\delta_{13} \equiv \ln Z_1 - \ln Z_3 = 0.62$ and $\delta_{34} \equiv \ln Z_3 - \ln Z_4 = 0.56$ in the heavy h_s scenario. The smallness of δ_{12} and δ_{34} reflects that the LZ experiment can not improve significantly the constraint of the XENON-1T experiment on the scenario, and the smallness of δ_{13} reflects that the XENON-1T experiment prefers slightly the $B_{\mu_X} \neq 0$ case to the $B_{\mu_X} = 0$ case.

- As for the other properties of the heavy h_s scenario, such as the range of the SI cross section, the correlation between Y_ν and $m_{\tilde{l}}$ and that between V_{11} and $m_{\tilde{l}}$, they are quite similar to those of the light h_s scenario. So we do not discuss them any more.

In summary, λ_ν is less constrained in the heavy h_s scenario than in the light h_s scenario, and the unitary constraint always plays an important role in limiting Y_ν except for the case of $B_{\mu_X} = 0$ and $Y_\nu > 0.2$, where the constraint from the LZ experiment is tighter than the unitary constraint in limiting Y_ν (see the last panel of Fig.8). We emphasize again that the moderately strong constraint of the DM DD experiments on the light h_s scenario with $B_{\mu_X} \neq 0$ comes from the fact that h_s is

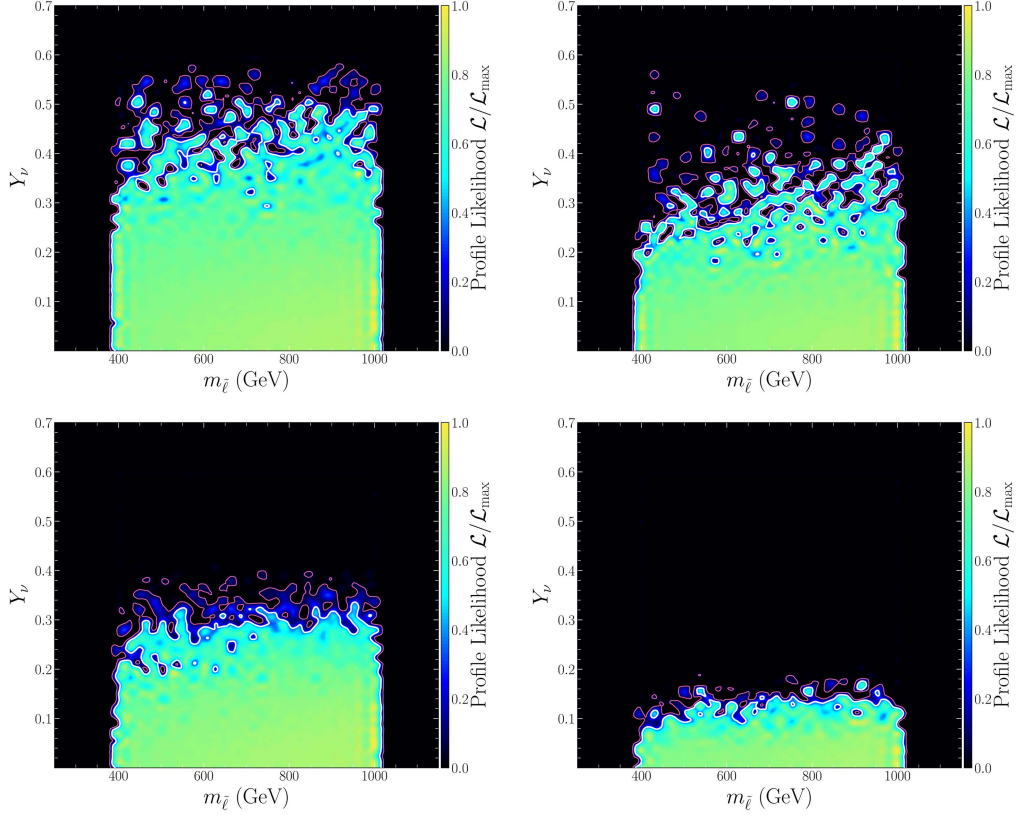


Figure 9. Same as Fig.4, but for the heavy h_s scenario defined in Table 1.

light and contains sizable doublet components so that the coupling $C_{\tilde{\nu}_1^* \tilde{\nu}_1 \text{Re}[S]}$ can contribute significantly to the scattering rate.

Finally, we point out that the most promising way to test the two scenarios at the LHC is to search for the Di- τ plus missing momentum signal through the process $pp \rightarrow \tilde{\chi}_1^\pm \tilde{\chi}_1^\mp \rightarrow (\tau^\pm E_T^{\text{Miss}})(\tau^\mp E_T^{\text{Miss}})$ [14, 15]. However, due to the small mass splitting between $\tilde{\chi}_1^\pm$ and $\tilde{\nu}_1$ in both scenarios, current LHC experiments are hardly to limit the parameter points in the 2σ CIs [15].

4 Conclusion

Motivated by the more and more stringent limitation of DM DD experiments on the traditional neutralino DM in natural MSSM and natural NMSSM, we augmented the NMSSM with the inverse seesaw mechanism to generate neutrino mass, and studied the feasibility that the lightest sneutrino acts as a DM candidate in our previous works [8, 14, 16]. One remarkable conclusion we obtained is that experimental constraints from both the DM search experiments and the collider experiments on the extension are generally relaxed in a great way, and consequently broad parameter spaces in the NMSSM which have been excluded by the experiments are resurrected

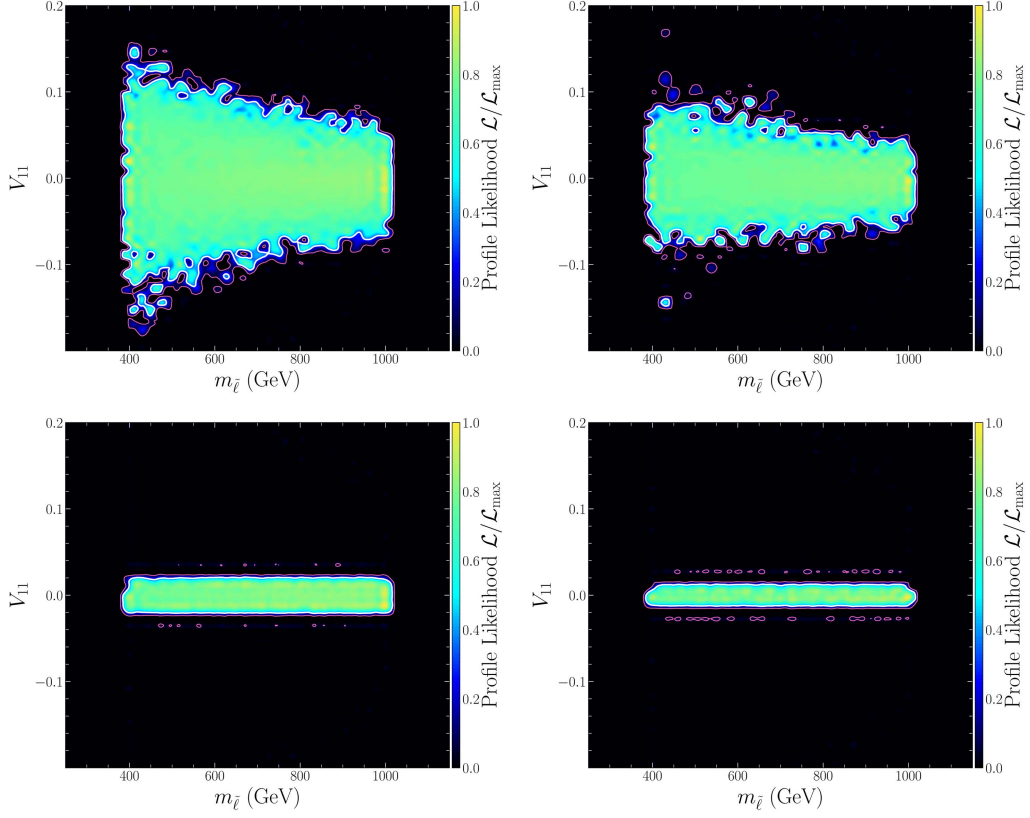


Figure 10. Same as Fig.5, but for the heavy h_s scenario defined in Table 1.

as experimentally allowed, especially the Higgsino mass may be around 100 GeV to predict Z -boson mass in a natural way. This makes the extension rather attractive and worthy of being studied carefully.

In this work, we realize that large neutrino Yukawa couplings λ_ν and Y_ν can enhance significantly the DM-nucleon scattering rate, so they may be limited by the recent XENON-1T experiment. We also realize that the upper bound on the unitary violation in neutrino sector sets certain correlation between the couplings λ_ν and Y_ν , which in return limits the parameter space of the ISS-NMSSM. Since these issues were not discussed before, we decide to study the impact of the leptonic unitary and current/future DM DD experiments on sneutrino DM sector. Explicitly speaking, we consider light h_s scenario and heavy h_s scenario by noting that the singlet dominated Higgs plays an important role in both DM annihilation and DM-nucleon scattering, and for each scenario we study $B_{\mu_X} \neq 0$ case and $B_{\mu_X} = 0$ case separately. The difference of the two cases comes from the fact that, besides the Higgs mediated contribution, Z boson also mediates the scattering of the DM with nucleons in the $B_{\mu_X} = 0$ case, and consequently the constraints of DM DD experiments in this case become much tighter than the $B_{\mu_X} \neq 0$ case.

In our study, we encode the constraints in a likelihood function, and perform

sophisticated scans over the vast parameter space of the model by Nested Sampling method. The results of our study may be summarized as follows:

- The XENON-1T experiment is able to set upper bound on the couplings λ_ν and Y_ν , and future LZ experiment can improve the bound significantly. The limitation is powerful when the state h_s is light and at same time contains sizable doublet components.
- As a useful complement to DM DD experiments, the unitary constraint always plays an important role in limiting Y_ν . It becomes more and more effective in this aspect when v_s approaches v from top to bottom.
- The parameter space favored by DM experiments shows a weak dependence on the left-handed slepton soft mass $m_{\tilde{l}}$. This implies that one may fix $m_{\tilde{l}}$ when he surveys the phenomenology of the DM sector by scanning intensively relevant parameters with the experimental constraints considered, and this does not affect the comprehensiveness of the results.
- The left-handed sneutrino component in the DM is tightly limited by the DM experiments, e.g. $|V_{11}| \lesssim 0.15$ for the $B_{\mu_X} \neq 0$ case and $|V_{11}| \lesssim 0.05$ for the $B_{\mu_X} = 0$ case if the sensitivity of current XENON-1T experiment is considered, and the upper bounds becomes 0.10 and 0.01 respectively once the sensitivity of future LZ experiment is reached.

Acknowledgement

This work is supported by the National Natural Science Foundation of China (NNSFC) under grant No. 11575053.

References

- [1] J. S. Hagelin, G. L. Kane and S. Raby, Nucl. Phys. B **241**, 638 (1984).
doi:10.1016/0550-3213(84)90064-6
- [2] G. Jungman, M. Kamionkowski and K. Griest, Phys. Rept. **267**, 195 (1996)
doi:10.1016/0370-1573(95)00058-5 [hep-ph/9506380].
- [3] T. Falk, K. A. Olive and M. Srednicki, Phys. Lett. B **339**, 248 (1994)
doi:10.1016/0370-2693(94)90639-4 [hep-ph/9409270].
- [4] C. Arina and N. Fornengo, JHEP **0711**, 029 (2007)
doi:10.1088/1126-6708/2007/11/029 [arXiv:0709.4477 [hep-ph]].
- [5] H. Baer, V. Barger and H. Serce, Phys. Rev. D **94**, no. 11, 115019 (2016)
doi:10.1103/PhysRevD.94.115019 [arXiv:1609.06735 [hep-ph]].

- [6] P. Huang, R. A. Roglans, D. D. Spiegel, Y. Sun and C. E. M. Wagner, *Phys. Rev. D* **95**, no. 9, 095021 (2017) doi:10.1103/PhysRevD.95.095021 [arXiv:1701.02737 [hep-ph]].
- [7] M. Badziak, M. Olechowski and P. Szczerbiak, *Phys. Lett. B* **770**, 226 (2017) doi:10.1016/j.physletb.2017.04.059 [arXiv:1701.05869 [hep-ph]].
- [8] J. Cao, L. Meng, Y. Yue, H. Zhou and P. Zhu, arXiv:1910.14317 [hep-ph].
- [9] H. Baer, V. Barger, P. Huang and X. Tata, *JHEP* **1205**, 109 (2012) doi:10.1007/JHEP05(2012)109 [arXiv:1203.5539 [hep-ph]].
- [10] J. Cao, Y. He, L. Shang, W. Su, P. Wu and Y. Zhang, *JHEP* **1610**, 136 (2016) doi:10.1007/JHEP10(2016)136 [arXiv:1609.00204 [hep-ph]].
- [11] J. Cao, Y. He, L. Shang, Y. Zhang and P. Zhu, *Phys. Rev. D* **99**, no. 7, 075020 (2019) doi:10.1103/PhysRevD.99.075020 [arXiv:1810.09143 [hep-ph]].
- [12] W. Abdallah, A. Chatterjee and A. Datta, *JHEP* **1909**, 095 (2019) doi:10.1007/JHEP09(2019)095 [arXiv:1907.06270 [hep-ph]].
- [13] U. Ellwanger, C. Hugonie and A. M. Teixeira, *Phys. Rept.* **496**, 1 (2010) doi:10.1016/j.physrep.2010.07.001 [arXiv:0910.1785 [hep-ph]].
- [14] J. Cao, X. Guo, Y. He, L. Shang and Y. Yue, *JHEP* **1710**, 044 (2017) doi:10.1007/JHEP10(2017)044 [arXiv:1707.09626 [hep-ph]].
- [15] J. Cao, J. Li, Y. Pan, L. Shang, Y. Yue and D. Zhang, *Phys. Rev. D* **99**, no. 11, 115033 (2019) doi:10.1103/PhysRevD.99.115033 [arXiv:1807.03762 [hep-ph]].
- [16] J. Cao, X. Jia, Y. Yue, H. Zhou and P. Zhu, arXiv:1908.07206 [hep-ph].
- [17] L. J. Hall, D. Pinner and J. T. Ruderman, *JHEP* **1204**, 131 (2012) doi:10.1007/JHEP04(2012)131 [arXiv:1112.2703 [hep-ph]].
- [18] U. Ellwanger, *JHEP* **1203**, 044 (2012) doi:10.1007/JHEP03(2012)044 [arXiv:1112.3548 [hep-ph]].
- [19] J. J. Cao, Z. X. Heng, J. M. Yang, Y. M. Zhang and J. Y. Zhu, *JHEP* **1203**, 086 (2012) doi:10.1007/JHEP03(2012)086 [arXiv:1202.5821 [hep-ph]].
- [20] J. Cao, F. Ding, C. Han, J. M. Yang and J. Zhu, *JHEP* **1311**, 018 (2013) doi:10.1007/JHEP11(2013)018 [arXiv:1309.4939 [hep-ph]].
- [21] U. Ellwanger and A. M. Teixeira, *JHEP* **1410**, 113 (2014) doi:10.1007/JHEP10(2014)113 [arXiv:1406.7221 [hep-ph]].
- [22] J. Cao, L. Shang, P. Wu, J. M. Yang and Y. Zhang, *Phys. Rev. D* **91**, no. 5, 055005 (2015) doi:10.1103/PhysRevD.91.055005 [arXiv:1410.3239 [hep-ph]].
- [23] J. Cao, L. Shang, P. Wu, J. M. Yang and Y. Zhang, *JHEP* **1510**, 030 (2015) doi:10.1007/JHEP10(2015)030 [arXiv:1506.06471 [hep-ph]].
- [24] J. Cao, Y. He, L. Shang, W. Su and Y. Zhang, *JHEP* **1608**, 037 (2016) doi:10.1007/JHEP08(2016)037 [arXiv:1606.04416 [hep-ph]].

- [25] U. Ellwanger and C. Hugonie, arXiv:1806.09478 [hep-ph].
- [26] M. J. Baker *et al.*, JHEP **1512**, 120 (2015) doi:10.1007/JHEP12(2015)120 [arXiv:1510.03434 [hep-ph]].
- [27] K. Griest and D. Seckel, Phys. Rev. D **43**, 3191 (1991). doi:10.1103/PhysRevD.43.3191
- [28] J. Cao, J. Lian, L. Meng, Y. Yue and P. Zhu, arXiv:1912.10225 [hep-ph].
- [29] E. Aprile *et al.* [XENON Collaboration], arXiv:1805.12562 [astro-ph.CO].
- [30] J. Baglio and C. Weiland, JHEP **1704**, 038 (2017) doi:10.1007/JHEP04(2017)038 [arXiv:1612.06403 [hep-ph]].
- [31] I. Gogoladze, N. Okada and Q. Shafi, Phys. Lett. B **672**, 235 (2009) doi:10.1016/j.physletb.2008.12.068 [arXiv:0809.0703 [hep-ph]].
- [32] A. Abada, G. Bhattacharyya, D. Das and C. Weiland, Phys. Lett. B **700**, 351 (2011) doi:10.1016/j.physletb.2011.05.020 [arXiv:1011.5037 [hep-ph]].
- [33] Z. Kang, J. Li, T. Li, T. Liu and J. M. Yang, Eur. Phys. J. C **76**, no. 5, 270 (2016) doi:10.1140/epjc/s10052-016-4114-9 [arXiv:1102.5644 [hep-ph]].
- [34] E. Bagnaschi *et al.*, Eur. Phys. J. C **78**, no. 3, 256 (2018) doi:10.1140/epjc/s10052-018-5697-0 [arXiv:1710.11091 [hep-ph]].
- [35] E. Fernandez-Martinez, J. Hernandez-Garcia and J. Lopez-Pavon, JHEP **1608**, 033 (2016) doi:10.1007/JHEP08(2016)033 [arXiv:1605.08774 [hep-ph]].
- [36] E. Arganda, M. J. Herrero, X. Marcano and C. Weiland, Phys. Rev. D **91**, no. 1, 015001 (2015) doi:10.1103/PhysRevD.91.015001 [arXiv:1405.4300 [hep-ph]].
- [37] J. Guo, Z. Kang, T. Li and Y. Liu, JHEP **1402**, 080 (2014) doi:10.1007/JHEP02(2014)080 [arXiv:1311.3497 [hep-ph]].
- [38] S. L. Chen and Z. Kang, Phys. Lett. B **761**, 296 (2016) doi:10.1016/j.physletb.2016.08.051 [arXiv:1512.08780 [hep-ph]].
- [39] J. Guo, Z. Kang, T. Li and Y. Liu, JHEP **1402**, 080 (2014) doi:10.1007/JHEP02(2014)080 [arXiv:1311.3497 [hep-ph]].
- [40] D. Barducci, G. Belanger, J. Bernon, F. Boudjema, J. Da Silva, S. Kraml, U. Laa and A. Pukhov, arXiv:1606.03834 [hep-ph].
- [41] G. Belanger, F. Boudjema, A. Pukhov and A. Semenov, Comput. Phys. Commun. **185**, 960 (2014) doi:10.1016/j.cpc.2013.10.016 [arXiv:1305.0237 [hep-ph]].
- [42] G. Belanger, F. Boudjema, C. Hugonie, A. Pukhov and A. Semenov, JCAP **0509**, 001 (2005) doi:10.1088/1475-7516/2005/09/001 [hep-ph/0505142].
- [43] J. R. Ellis, K. A. Olive and C. Savage, Phys. Rev. D **77**, 065026 (2008) doi:10.1103/PhysRevD.77.065026 [arXiv:0801.3656 [hep-ph]].
- [44] J. M. Alarcon, J. Martin Camalich and J. A. Oller, Phys. Rev. D **85**, 051503 (2012) doi:10.1103/PhysRevD.85.051503 [arXiv:1110.3797 [hep-ph]].

- [45] X. L. Ren, L. S. Geng and J. Meng, Phys. Rev. D **91**, no. 5, 051502 (2015) doi:10.1103/PhysRevD.91.051502 [arXiv:1404.4799 [hep-ph]].
- [46] X. Z. Ling, X. L. Ren and L. S. Geng, Phys. Lett. B **783**, 7 (2018) doi:10.1016/j.physletb.2018.05.063 [arXiv:1710.07164 [hep-ph]].
- [47] J. M. Alarcon, L. S. Geng, J. Martin Camalich and J. A. Oller, Phys. Lett. B **730**, 342 (2014) doi:10.1016/j.physletb.2014.01.065 [arXiv:1209.2870 [hep-ph]].
- [48] B. Dumont, G. Belanger, S. Fichet, S. Kraml and T. Schwetz, JCAP **1209**, 013 (2012) doi:10.1088/1475-7516/2012/09/013 [arXiv:1206.1521 [hep-ph]].
- [49] P. Bechtle, S. Heinemeyer, O. Stål, T. Stefaniak and G. Weiglein, JHEP **1411**, 039 (2014) doi:10.1007/JHEP11(2014)039 [arXiv:1403.1582 [hep-ph]].
- [50] P. Bechtle, S. Heinemeyer, O. Stal, T. Stefaniak and G. Weiglein, Eur. Phys. J. C **75**, no. 9, 421 (2015) doi:10.1140/epjc/s10052-015-3650-z [arXiv:1507.06706 [hep-ph]].
- [51] D. S. Akerib *et al.* [LUX-ZEPLIN Collaboration], arXiv:1802.06039 [astro-ph.IM].
- [52] N. Aghanim *et al.* [Planck Collaboration], arXiv:1807.06209 [astro-ph.CO].
- [53] S. Matsumoto, S. Mukhopadhyay and Y. L. S. Tsai, Phys. Rev. D **94** (2016) no. 6, 065034 doi:10.1103/PhysRevD.94.065034 [arXiv:1604.02230 [hep-ph]].
- [54] L. M. Carpenter, R. Colburn, J. Goodman and T. Linden, Phys. Rev. D **94**, no. 5, 055027 (2016) doi:10.1103/PhysRevD.94.055027 [arXiv:1606.04138 [hep-ph]].
- [55] X. J. Huang, C. C. Wei, Y. L. Wu, W. H. Zhang and Y. F. Zhou, Phys. Rev. D **95**, no. 6, 063021 (2017) doi:10.1103/PhysRevD.95.063021 [arXiv:1611.01983 [hep-ph]].
- [56] M. Ackermann *et al.* [Fermi-LAT Collaboration], Phys. Rev. Lett. **115**, no. 23, 231301 (2015) doi:10.1103/PhysRevLett.115.231301 [arXiv:1503.02641 [astro-ph.HE]].
- [57] see website: www-glast.stanford.edu/pub_data/1048
- [58] F. Feroz, M. P. Hobson and M. Bridges, Mon. Not. Roy. Astron. Soc. **398**, 1601 (2009) doi:10.1111/j.1365-2966.2009.14548.x [arXiv:0809.3437 [astro-ph]].
- [59] F. Feroz, M. P. Hobson, E. Cameron and A. N. Pettitt, arXiv:1306.2144 [astro-ph.IM].
- [60] A. Fowlie and M. H. Bardsley, Eur. Phys. J. Plus **131**, no. 11, 391 (2016) doi:10.1140/epjp/i2016-16391-0 [arXiv:1603.00555 [physics.data-an]].
- [61] F. Staub, Comput. Phys. Commun. **185**, 1773 (2014) doi:10.1016/j.cpc.2014.02.018 [arXiv:1309.7223 [hep-ph]].
- [62] F. Staub, Comput. Phys. Commun. **184**, 1792 (2013) doi:10.1016/j.cpc.2013.02.019 [arXiv:1207.0906 [hep-ph]].
- [63] F. Staub, arXiv:0806.0538 [hep-ph].
- [64] W. Porod and F. Staub, Comput. Phys. Commun. **183**, 2458 (2012) doi:10.1016/j.cpc.2012.05.021 [arXiv:1104.1573 [hep-ph]].

- [65] G. Belanger, F. Boudjema, A. Pukhov and A. Semenov, *Comput. Phys. Commun.* **185**, 960 (2014) doi:10.1016/j.cpc.2013.10.016 [arXiv:1305.0237 [hep-ph]].
- [66] S. Chang, R. Edezhath, J. Hutchinson and M. Luty, *Phys. Rev. D* **89**, no. 1, 015011 (2014) doi:10.1103/PhysRevD.89.015011 [arXiv:1307.8120 [hep-ph]].
- [67] A. Berlin, D. Hooper and S. D. McDermott, *Phys. Rev. D* **89**, no. 11, 115022 (2014) doi:10.1103/PhysRevD.89.115022 [arXiv:1404.0022 [hep-ph]].
- [68] P. Gregory, *Bayesian Logical Data Analysis for the Physical Sciences*. Cambridge University Press, 2005.
- [69] H. Jeffreys (1961). *The Theory of Probability* (3rd ed.). Oxford. p. 432.
- [70] F. Feroz, B. C. Allanach, M. Hobson, S. S. AbdusSalam, R. Trotta and A. M. Weber, *JHEP* **0810**, 064 (2008) doi:10.1088/1126-6708/2008/10/064 [arXiv:0807.4512 [hep-ph]].
- [71] M. Kakizaki, A. Santa and O. Seto, *Int. J. Mod. Phys. A* **32**, no. 10, 1750038 (2017) doi:10.1142/S0217751X17500385 [arXiv:1609.06555 [hep-ph]].